Nonlinear Normal Mode Backbone Estimation with Near-Resonant Steady State Inputs

Michael Kwarta and Matthew S. Allen

University of Wisconsin - Madison, Department of Engineering Mechanics
1500 Engineering Drive, Engineering Research Building, Madison, WI 53706, USA
Email address: kwarta@wisc.edu (Michael Kwarta); matt.allen@wisc.edu (Matthew S. Allen)

Abstract

This work presents a new technique for nonlinear system identification that utilizes near-resonant steady-state harmonically excited vibration measurements to estimate the Nonlinear Normal Mode backbones. The algorithm is based on the previously proposed Single Nonlinear Resonant Mode formula and uses it in a new and more effective way to estimate one point on the nonlinear mode from only one steady-state measurement collected near the resonance. A by-product of this work is a derivation of a novel formula expressing how the damping ratio changes with the motion amplitude. Several measurements at various forcing amplitudes can be combined to estimate the nonlinear mode and damping as a function of amplitude, which can be further used to predict the forced steady-state response of the structure in the vicinity of the mode of interest. Compared to existing phase resonance methods, the proposed technique can reduce the time required to obtain measurements and avoids difficulties due to e.g. the premature jump phenomenon. The algorithm assumes that the modes are well-separated and no internal resonances are present in the system. Additionally, it requires the accurate identification of linear modes in the low-amplitude vibration tests and it assumes that the nonlinear normal mode shape does not change significantly with response amplitude. The method is first evaluated numerically using reduced models of clamped-clamped flat and curved beams that exhibit both stiffening and softening-stiffening responses, respectively. Then the method is employed experimentally to measure the NNM backbones of beams that were manufactured from polylactide using a 3D printer and experience significant eigen-frequency shifts when the motion amplitude increases. The results are validated against measurements collected using the traditional phase resonance testing approach.

Keywords: Nonlinear System Identification, Single Nonlinear Resonant Mode Formula, Nonlinear Normal Mode Estimation, Phase-Resonance Testing, Nonlinear Experimental Dynamics

1. Introduction

The vast majority of industrial structural dynamic systems are still modeled and designed as linear. The reason for this preference is that the theory behind this class of mechanical systems is well understood and many powerful tools are available for their analysis. When a nonlinear characteristic is encountered in an industrial structure, it is a common practice to approximate it locally with a linear model, i.e. to adjust the linear parameters to reflect the nonlinear behavior. However, there are still cases where the nonlinearity present in the system is either ignored or the structure is redesigned such that the nonlinear phenomena migrate out of the operating range.

Understanding the nonlinear nature of certain mechanical systems can bring invaluable benefits to the engineering design and modeling processes. Recent works show that approaching the problems from this angle can be helpful in e.g. reduction of the nonlinear vibrations [1, 2] or modeling systems whose responses/failures cannot be understood using linear vibration theory [3, 4]. Moreover, a demand for strong and stiff enough structures, yet efficient from the material and weight standpoints, is lately observed in the industry. Designing such mechanical systems might not be achieved solely with the linear approach, thus the significance of going beyond the standard vibration analysis has been recently increasing.

1.1. Nonlinear Normal Modes

The response of an oscillating linear system can be expressed as a combination of its linear modes. This is possible due to their mutual orthogonality, which can be further used to diagonalize the matrices describing the mass and stiffness distributions. Additionally, this property implies that the natural frequencies are vibration-level-independent. In other words, the maximum points of the response functions (RFs) calculated for different force levels lay one above/below another forming a straight vertical line on an amplitude vs. frequency chart, as indicated in Fig. 1a.

The principle of superposition (by definition) does not apply to *nonlinear* systems, since their natural frequencies can shift with the motion amplitude. They can exhibit a softening (stiffening) characteristic when the nonlinear eigen-frequency decreases (increases) with the vibration level – which is usually expressed either with the displacement amplitude or the

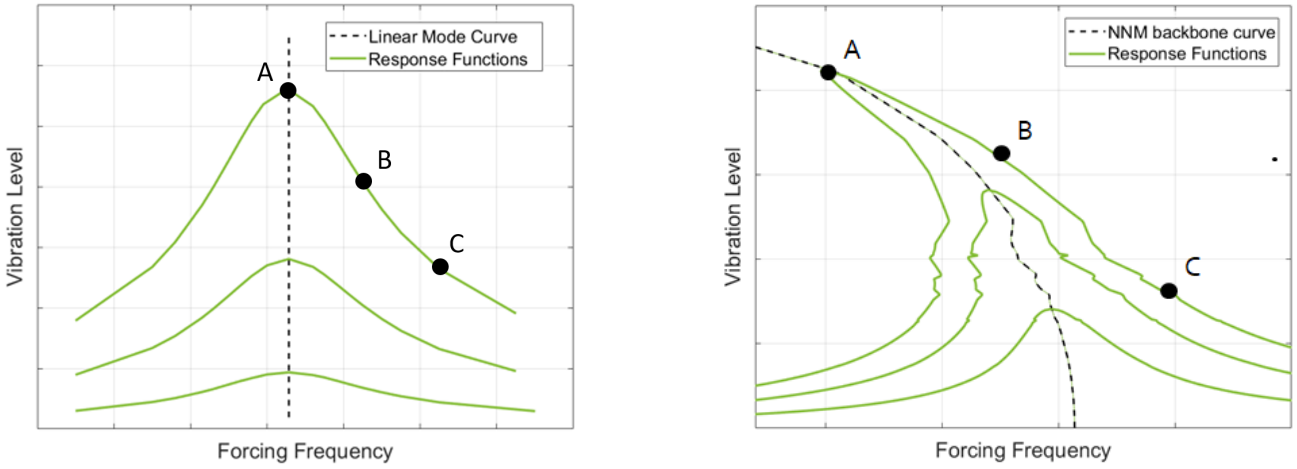

(a) **(b)**

Fig. 1: Examples of response functions of **(a)** linear and **(b)** nonlinear systems obtained for different forcing levels. Parts of these response functions can be measured with the Phase Tuning method, which allows for collecting the steady-state response of the structure via controlling the frequency and amplitude of applied force.

energy accumulated in the oscillating system. An example of the softening characteristic is presented in Fig. 1b. The figure also shows the natural frequency as a function of vibration level, which is called the Nonlinear Normal Mode (NNM) curve.

The concept of an NNM was first introduced by Rosenberg in the 1960s [5, 6, 7, 8], where it was defined as any type of *vibration in unison* of a conservative nonlinear system (a synchronous oscillation). After approximately 30 years of being considered only in the theoretical realm [9, 10, 11, 12, 13, 14, 15], the Nonlinear Normal Modes experienced their second youth in 1990s thanks to the work of Vakakis et al. [16, 17, 18], as well as Shaw and Pierre [19, 20] who extended the NNM concept to damped systems. Since the motion is still periodic even in the presence of internal resonances, the original Rosenberg definition of an NNM has been generalized to include a (not-necessarily synchronous) periodic motion of the conservative system [21]. In other words, any periodic motion of a conservative nonlinear system is considered to be an NNM.

Nonlinear system identification and further prediction of the structure's motion is a complex effort because of a large variety of input types, force levels and distributions, etc. that must be considered. If one can show that the measured NNMs correspond well with those from a simulation model, then one can make some powerful statements about the applicability of the model over a certain range of vibration amplitudes. There are many theoretical, numerical and experimental methods available, which help in extracting the NNM based on particular input data. The most basic approaches are based on phase-resonance testing, which is described in the following subsection. The algorithm proposed in this work can be classified – according to [22] – as a modal method, hence the in-depth overview of the algorithms of this type is provided in subsection 1.3.

1.2. Phase Resonance Testing

Phase Tuning (also known as Phase-Resonance Testing) is a well known experimental technique for both linear and nonlinear structures. Since the method provides very accurate measurements of the structure's damping and is robust in the presence of nonlinearities, it is frequently used in e.g. ground vibration testing [23], which is one of the critical tests performed during aircraft development. In the case studies presented in this article, the experimental measurements (including those collected in the numerical simulations) are generated using the single input (one shaker) Phase Tuning approach.

When using the phase resonance method, the structure is excited harmonically until it reaches *steady-state*, and then the amplitude and/or frequency of the applied forcing signal is adjusted until the structure is resonant in the mode of interest. If the force amplitude is kept constant then the forcing frequency can be adjusted in order to bring the vibrating structure to its resonance. In other words – if the forcing amplitude is fixed, one could adjust the frequency to march up a branch of a linear or nonlinear Response Function, as shown in Fig. 1 in the path that starts from point C, through B, ending at point A.

While Phase-Resonance testing has long been used for linear systems, Peeters et al. [24] recently showed that one can use it to measure a system's undamped Nonlinear Normal Modes [25]. Here we vary from their derivation to also provide background on the SNRM method presented in [26]. Consider a multi-degree-of-freedom (MDOF) nonlinear equation of motion (EOM) of certain structure, represented here with Eq. (1).

$$\mathbf{M}\ddot{\mathbf{x}} + \mathbf{K}\mathbf{x} + \mathbf{f}_{nl}(\mathbf{x}) + \mathbf{g}_{nl}(\dot{\mathbf{x}}) = \mathbf{f}(t), \tag{1}$$

where $\mathbf{M}$ and $\mathbf{K}$ are the matrices modeling respectively the mass and linear stiffness distribution in the mechanical system, $\mathbf{x}(t)$ is the displacement response of the structure excited with the force signal $\mathbf{f}(t)$. The quantities $\mathbf{f}_{nl}$ and $\mathbf{g}_{nl}$ represent, respectively, the nonlinear restoring and dissipative forces present in the system. Note that the nonlinearities are presumed to depend only on the displacements or velocities with no cross terms so that the undamped NNMs exist and the quadrature condition introduced later can be satisfied. However, strictly speaking the SNRM function may be valid for more general cases than shown here.

Equation (1) can be expressed in terms of the modal coordinates by applying the linear modal transformation (2) and left-multiplying the equation with the matrix $\mathbf{\Phi}^T$. The transformed EOM is presented in Eq. (3).

$$\mathbf{x} = \mathbf{\Phi}\mathbf{q} \tag{2}$$

$$\ddot{\mathbf{q}} + \begin{bmatrix} \ddots & & \\ & \omega_{0,k}^2 & \\ & & \ddots \end{bmatrix} \mathbf{q} + \boldsymbol{\theta}_{nl}(\mathbf{q}) + \boldsymbol{\gamma}_{nl}(\dot{\mathbf{q}}) = \mathbf{\Phi}^T \mathbf{f}(t), \tag{3}$$

where: $\mathbf{q}(t)$ is the vector of modal coordinates, $\omega_{0,k}$ is the natural frequency of the k-th linear mode and the columns of matrix $\mathbf{\Phi}$ are the mass-normalized eigen-shapes of the linearized, undamped and homogeneous equation (1). The vectors $\boldsymbol{\theta}_{nl}$ and $\boldsymbol{\gamma}_{nl}$ are the nonlinear parts of the modal EOM, and consist of the stiffness and damping terms, respectively. Naturally, $\boldsymbol{\theta}_{nl}(\mathbf{q}) = \mathbf{\Phi}^T \mathbf{f}_{nl}(\mathbf{\Phi}\mathbf{q})$ and $\boldsymbol{\gamma}_{nl}(\dot{\mathbf{q}}) = \mathbf{\Phi}^T \mathbf{g}_{nl}(\mathbf{\Phi}\dot{\mathbf{q}})$.

The nonlinear modal equations of motion (3) are in general coupled with one another by the nonlinear stiffness and dissipative terms. The most straightforward way to derive the SNRM method is to assume that the nonlinear coupling terms in Eq. (3) are negligible, in which case the modal equations can be simplified as follows Eq. (4) .

$$\ddot{q}_j + \omega_{0,j}^2 q_j + \theta_{nl,j}(q_j) + \gamma_{nl,j}(\dot{q}_j) = \mathbf{\Phi}_j^T \mathbf{f}(t) \tag{4}$$

Note that the SNRM equations that will be presented in Sec. 2 are derived using the method of averaging [27] and so one could alternatively assert that the coupling terms were negligible in an averaged sense, relaxing this assumption somewhat.

The nonlinear modal equation of motion (4) can be further split *at resonance* into Eqs. (5). This is because (at resonance) the harmonics of the inertia and linear as well as nonlinear stiffness terms are 90 degrees out of phase with the corresponding harmonics of the damping and forcing signals [28]. When this occurs, the resulting response is clearly a Nonlinear Normal Mode, since it is a solution of the conservative nonlinear EOM. Indeed, equation (5a) represents motion of such system, while (5b) shows that the forcing and velocity signals are synchronized at resonance, which is often called a (nonlinear) phase quadrature criterion [24].

$$\begin{cases} \ddot{q}_j + \omega_{0,j}^2 q_j + \theta_{nl,j}(q_j) = 0 & \text{(5a)} \\ \gamma_{nl,j}(\dot{q}_j) = \mathbf{\Phi}_j^T \mathbf{f}(t) & \text{(5b)} \end{cases}$$

The property (5b) is utilized in the Phase Tuning method to determine how far the oscillating system is from its resonance. Namely, when the structure vibrates at its natural frequency – a straight line is seen in the force vs. velocity plot. In contrast, if the response of a *linear* system is near but not exactly at the eigen-frequency then the plot will show an ellipse. The larger the ellipse is the further the structure is from the resonance, as illustrated in Figs. 2a-c. When it comes to the Phase Resonance Testing of a nonlinear system, the loop can have a more complex shape, as e.g. presented in Figs. 2d-f. This is because the requirement stated in Eq. (5b) is usually difficult and tedious to satisfy directly, since there might be e.g. multiple sub- or super-harmonics present in the system's response. However, the Phase Tuning approach combined with certain clever concepts can still be a convenient and reliable tool to estimate how close the structure is to its nonlinear resonance. An in-depth description of one such concept, called the NNM Appropriation Indicator (NNMAI), is provided later in this article.

Phase-Resonance Testing is a simple and effective method for testing nonlinear structures, yet there is one important drawback. While marching up the nonlinear Response Function curve, the mechanical system will often fall off of the stable branch before reaching the actual turning point (marked with A in Fig. 1b). This is called the *premature jump phenomenon* [29] and it can greatly increase the time required for testing (e.g. see Sec. 4 for further discussion). Since the NNM backbone is often a border between the regions of stable and unstable motion, as one approaches the resonance even a slight perturbation can nudge the system from the stable region. Control-based techniques, such as phase locked loop (PLL) [30] or control-based continuation (CBC) [31] can stabilize the system and prevent premature jump, and can greatly accelerate measurements. However, these techniques require hardware with feedback control capability; most vibration test equipment does not have this capability and systems that do have it often have lower bandwidths than comparable open-loop acquisition systems.

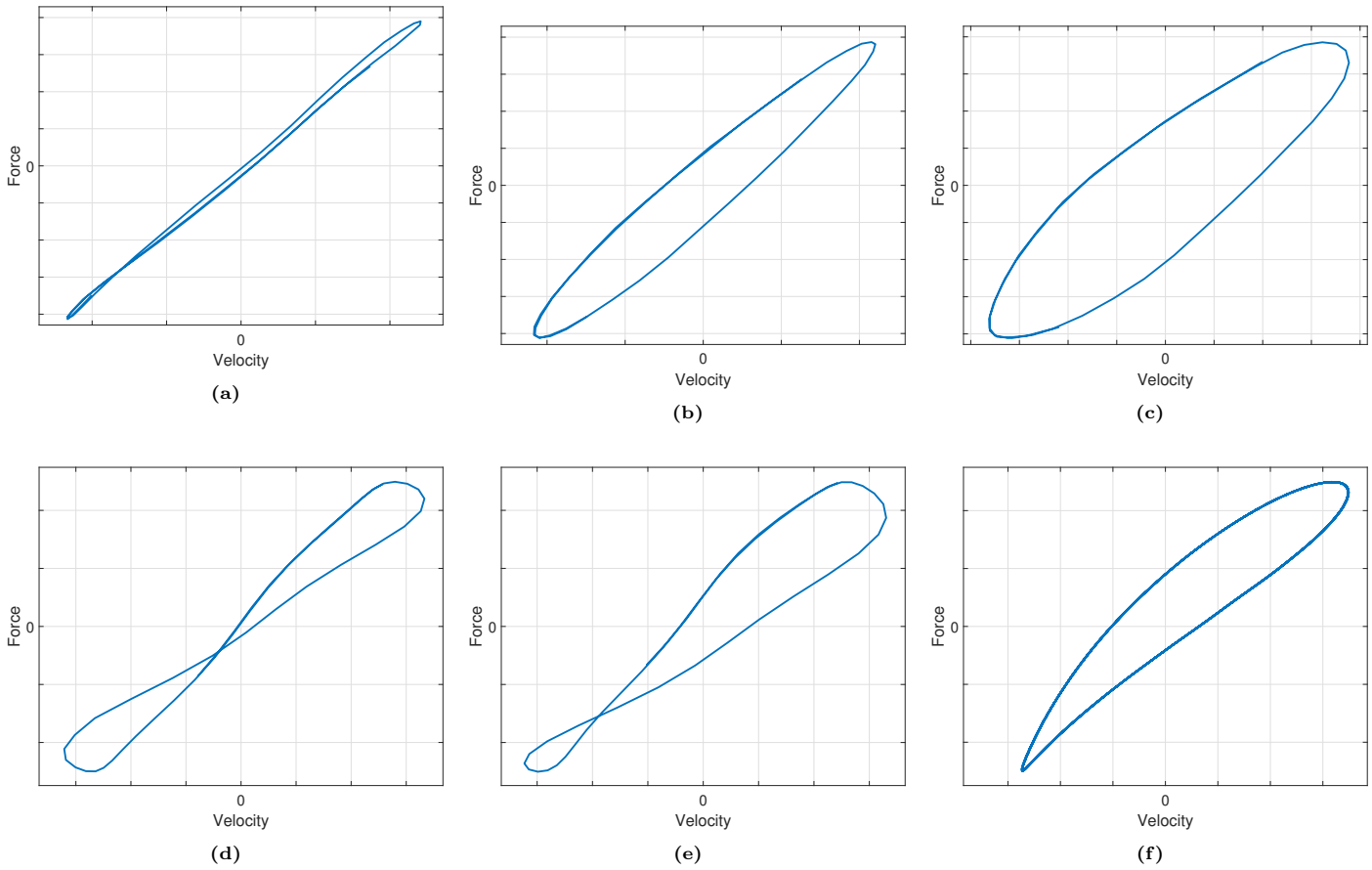

Fig. 2: The Phase Tuning method compares force and velocity signals to indicate whether the system oscillates at its resonance. Subplots **(a)**, **(b)** and **(c)** correspond to points **A**, **B** and **C** shown in Fig. 1a. Subplots **(d)**, **(e)** and **(f)** illustrate examples of the steady-state responses that are possible between points **A** and **B** on chart 1b.

Additionally, one must tune the control gains to stabilize the system near the resonance, which may require significant trial and error while exciting the system at high amplitudes. On the other hand, when control-based methods are applicable, they tend to be very fast as one can march up the NNM automatically. They may also stabilize systems that exhibit period-doubling or quasi-periodic response. It is worth noting that the method proposed here could be combined with a control-based technique to obtain the best of both worlds. One could use control-based continuation to measure the resonant response near an NNM, but far enough away to avoid the bifurcation point, and then use the SNRM approach proposed here to estimate the NNM from those measurements. For the present study the authors did not have access to a suitable closed-loop system, but such an approach will be considered in future works.

Another often-encountered issue of Phase-Resonance Testing is the feedback of the oscillating structure, which usually leads to distortions of the input force signal and can impact the measurements quality. Naturally, the closer the structure is to its resonance the larger the feedback is, lowering the quality of the data collected. Moreover, precise Phase Tuning measurements are often time consuming, as one must wait for steady-state at each point and then can only capture the steady-state response for a single forcing amplitude and frequency at a time. If measurements are needed in a wider range of frequencies or amplitudes, then the testing can become lengthy.

1.3. Nonlinear System Identification with Modal Methods

Modal methods seek to identify the nonlinear eigen-properties of the mechanical system, which can be further used to approximate the solution to the nonlinear equation of motion, rather than trying to fit a differential equation to the measurements (or to approximate the form of the nonlinear EOM). They are usually based on a frequency domain description and thus require providing steady-state measurements.

Some of the modal methods used today are based on the Single Nonlinear Resonant Mode (SNRM) concept proposed by Szemplińska-Stupnicka in [26]. The nonlinearity is introduced there via expressing the natural frequency, damping ratio and (possibly) mode shape as functions of the vibration level. The SNRM-based method, in its original formulation, can only be applied when the modes are well-separated and no internal resonances occur.

One of the previously proposed system identification procedures based on the SNRM model function is implemented in the COde for Nonlinear identifiCation from mEasured Response To vibratiOn, also known as CONCERTO [32]. The software was successfully employed in estimating the nonlinear characteristics exhibited by anti-vibration mounts [33] and a mechanical system replicating the complexity of a typical helicopter structure [32]. CONCERTO requires finding the steady-state response at two points on a response function for a single vibration amplitude of the mode in question. That can be limiting because the measurements must be taken on both sides of the Nonlinear Normal Mode backbone. However, one of these sides is often on an unstable branch when the motion amplitude is high enough. Hence, the applicability of the concept is narrowed to systems exhibiting very small natural frequency shifts.

Another example of a modal method can be found in the work of Arslan and Özgüven [34], where the nonlinear properties of a cantilever beam with a cubic spring attached to its end were identified. The method presented there is limited to structures with a single nonlinear element whose location must be known a priori. The Response-Controlled Stepped-Sine Testing (RCT) proposed by Karaağaçli and Özgüven in [35] and further elaborated in [36, 37] is an extension of the method presented in [34].

The RCT approach is based on the quasi-linearization of the multi-degree of freedom nonlinear systems obtained via keeping the displacement amplitude of the driving point constant. The nonlinear parameters are identified as functions of the modal amplitude by applying standard linear modal analysis techniques to the measured controlled-amplitude Response Functions. The identified nonlinear modal parameters can then be used in the Single Nonlinear Resonant Mode formula to synthesize near-resonant nonlinear RFs (including unstable branches). The RCT method can also be used to extract the nonlinear Response Functions with accurately measured turning points and unstable branches, not only from the identified modal model, but also directly from the experiment via the Harmonic Force Surface (HFS) concept [35]. Hence, it allows for extracting the NNM backbone curves of strongly nonlinear systems.

The method was successfully applied to identify a T-beam benchmark with strong cubic stiffness and a real missile with considerable damping nonlinearity due to bolted connections [35], as well as to a double clamped beam with strong geometrical (distributed) nonlinearity in [36]. In [37], the authors employed the RCT technique to identify the NNM backbone curves of the T-beam and a real control fin actuation mechanism that exhibits strong and complex nonlinear behavior due to backlash and friction.

The Single Nonlinear Resonant Mode model function is also employed in the validation process of the algorithms presented in e.g. [30] or [38]. In the former case, the authors measure the NNM backbone using an automated phase-controlled tracking algorithm. In the latter, the system is identified using the Polynomial Nonlinear State-Space (PNLSS) algorithm [39, 40, 41] with an assumption that the nonlinear damping ratio can be computed by equating the energy input into the system with the dissipated energy averaged over one cycle. It is worth noting that the phase-control tracking is not the only algortihm that can be employed in the automatic NNM backbone measurements. Another recently developed technique, called Control-Based Continuation (CBC) also allows for the nonlinear mechanical systems testing in a controlled fashion. In [31], the authors used this approach to identify a backbone curve of a SDOF nonlinear oscillator and compared their findings with those extracted using the resonant-decay method.

1.4. Objectives and Contributions

The objective of this article is to propose a new algorithm based on the Single Nonlinear Resonant Mode model function, which can be used to identify the NNM backbones of nonlinear structures and to reconstruct the near-resonant response. This work builds on that in [30] where Peter, Scheel et al. measured the NNM directly with a control-phase tracking approach. Then, they used the SNRM formula together with the obtained NNM curve to compute the Response Functions in its vicinity. The strategy presented here is reverse. We utilize the SNRM function to find the NNM backbone using a near-resonant measurements. Hence, the method presented in this work is called *the inverse SNRM-based algorithm*. Moreover, in [30] the SNRM algorithm is combined with a model evaluating the nonlinear damping based on the power dissipated. In this work, we propose a novel expression to model the effective damping, which is derived directly from the SNRM function and hence is automatically compatible with any SNRM-based technique.

Therefore, the main contribution of this work is to show that the SNRM formula can be used to estimate the location of a nonlinear resonant point using only *one* near-resonant steady-state measurement and to demonstrate the method experimentally. The algorithm proposed here speeds up the testing process as one does not need to take the time to tune the structure exactly to the resonance. Additionally, since one is not trying to test very close to the resonance, the system is less likely to fall off of the stable branch – a phenomenon that often slows down this type of testing. Furthermore, we use the identified NNM backbones to estimate the nonlinear Response Functions near of the resonance and compare them with those measured experimentally. This validates the results and allows the reader to see the limits of the applicability of the SNRM formula for the structures studied here.

The following section presents the theory behind the algorithm proposed and explains the nonlinear system identification process. In section 3, the method is tested in simulated experiments by applying it to ICE-ROMs of flat and curved beams,

and the outcomes are validated and discussed. Section 4 presents the results from the identification attempt performed on beams 3D-printed from polylactide acid. Finally, section 5 presents conclusions and future work.

2. Algorithm Overview

2.1. Theoretical Background

This section begins with a derivation of the approximate solution to the nonlinear equation of motion of the oscillating system. The solution shows that the natural frequencies and modal damping ratios of the structure might change with the vibration amplitude. This observation will later serve as an argument to postulate the Single Nonlinear Resonant Mode (SNRM) formula, which is the basis of the algorithm presented here. The derivation starts with Eq. (4) obtained in section 1.2.

Suppose that the mechanical system is excited with a sinusoidal forcing signal, Eq. (6a), and that the steady-state response is well approximated with a single harmonic as in Eq. (6b).

$$\mathbf{f}(t) = \mathrm{Re}\{-i\mathbf{F}e^{i\Omega t}\} \qquad\qquad q_j(t) = \mathrm{Re}\{\hat{Q}_j e^{i\Omega t}\}, \tag{6}$$

where Ω is the forcing frequency, $\mathbf{F}$ is the force distribution (constant and *real* vector), $\hat{Q}_j$ is the unknown complex amplitude of the j-th modal coordinate and $Q_j = |\hat{Q}_j|$. From a practical stand-point, including the tests presented later in this article, one would at least hope that the excitation frequency is dominant in the system's response. In order to use the SNRM approach, we have to also assume that the modal coupling is negligible, in which case the eigen-shape of the dominant mode will not change significantly with increasing vibration level, as indicated in Eq. (7).

$$\frac{\partial \mathbf{\Phi}_j}{\partial Q_j} \approx \mathbf{0} \tag{7}$$

Approximate analytical methods (such the averaging method [42]) can be employed in finding an explicit form of the quantity $\hat{Q}_j$. The results obtained with the method of averaging are presented in Eqs. (8) and (9).

$$\hat{Q}_j = Q_j e^{i(\varphi_j - \frac{\pi}{2})} \qquad Q_j = \frac{\mathbf{\Phi}_j^T \mathbf{F}}{\sqrt{\left[(\omega_{0,j} + \Delta\omega_{0,j})^2 - \Omega^2\right]^2 + \Omega^2 \delta_j^2}} \qquad \varphi_j = \tan^{-1}\left(\frac{\Omega\delta_j}{(\omega_{0,j} + \Delta\omega_{0,j})^2 - \Omega^2}\right), \tag{8}$$

and

$$\Delta\omega_{0,j}(Q_j) = \frac{1}{2\pi\omega_{0,j}Q_j}\int_0^{2\pi} \theta_{nl,j}\left(Q_j\cos(\beta)\right)\cos(\beta)d\beta \tag{9a}$$

$$\delta_j(Q_j) = \frac{1}{2\pi\omega_{0,j}Q_j}\int_0^{2\pi} \gamma_{nl,j}\left(-Q_j\Omega\sin(\beta)\right)\sin(\beta)d\beta \tag{9b}$$

The new quantities introduced in Eqs. (8) and (9) are: φ_j – the phase angle of the displacement response (determined with respect to the phase of the input signal) as well as $\delta_j(Q_j)$ and $\Delta\omega_{0,j}(Q_j)$, which stand for – respectively – the nonlinear modal damping ratio and correction to the linear natural frequency of the j-th mode. As indicated in Eq. (9), these two *"corrections"* depend on the vibration amplitude.

The approximate solution, presented in (8), and the fact that the eigen-frequency and modal damping ratio change with the motion amplitude serve as two base observations in postulating the more practical (from the system ID view-point) solution form to the nonlinear EOM (1). This expression – shown in Eq. (10) – is called the Single Nonlinear Resonant Mode (SNRM) function and was first proposed in [26]. The SNRM formula is expressed below in terms of the velocity, since in the case studies presented later in this article the velocity response of the structure was measured.

$$\mathbf{v}(t) = \mathrm{Re}\{\mathbf{V}^{meas}e^{i\Omega t}\} \tag{10a}$$

$$\mathbf{V}^{meas} \approx \mathbf{V}^{model} = \underbrace{\sum_{k=1}^{N_{RB}} \frac{-\mathbf{\Phi}_k^{RB}\left(\mathbf{\Phi}_k^{RB}\right)^T\mathbf{F}}{\Omega}}_{\mathbf{V}^{RB}} + \underbrace{\frac{\mathbf{\Phi}_j\mathbf{\Phi}_j^T\mathbf{F}\Omega}{\tilde{\omega}_{0,j}^2 - \Omega^2 + 2i\tilde{\zeta}_j\tilde{\omega}_{0,j}\Omega}}_{\mathbf{V}_j^{nl}} + \underbrace{\sum_{\substack{k=1\\k\neq j}}^{N_{lin}} \frac{\mathbf{\Phi}_k\mathbf{\Phi}_k^T\mathbf{F}\Omega}{\omega_{0,k}^2 - \Omega^2 + 2i\zeta_k\omega_{0,k}\Omega}}_{\mathbf{V}_j^{lin}}, \tag{10b}$$

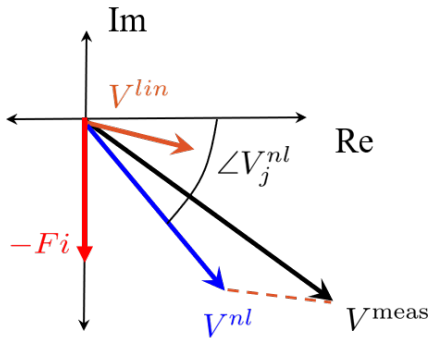

Fig. 3: Visualization of quantities from equations (6a) and (11–13)

where: $\mathbf{v}(t)$ stands for the experimentally measured full-field velocity response; Ω is the forcing frequency; $\mathbf{\Phi}_i$, $\omega_{0,i}$, ζ_i are, respectively, the mass-normalized mode shape, natural frequency and modal damping ratio of the i-th mode; $\mathbf{F}$ is the already mentioned distribution of a sinusoidal force excitation; $\mathbf{\Phi}_i^{RB}$ is the i-th rigid body mode; j is the index of the dominant mode, and N_{lin} and N_{RB} denotes the number of relevant linear and rigid body modes, respectively. The quantities marked ($\sim$) vary with the vibration level.

The objective of this work is to propose an algorithm, based on the model function (10), that allows for identification of nonlinear structures. The strengths of the SNRM formula are: (i) an explicit mathematical form of the system's *steady-state* response and (ii) a straight-forward correlation to the linear vibration theory. Indeed, the response of the oscillating linear system can be expressed as a sum of its linear modes. If we look at the SNRM function from this angle, we could state that it extracts one of the sum components and models it as nonlinear, while keeping the remaining modes superimposed linearly.

As presented in Eq. (10), the nonlinearity is modeled via representing two physical properties – $\omega_{0,j}$ and ζ_j – as functions of the motion amplitude. In this work, the vibration level is expressed with the velocity amplitude of a specific point on the oscillating object. Thus, instead of looking into the full-field response of the system ($\mathbf{V}^{meas}$, $\mathbf{V}_j^{nl}$, $\mathbf{V}_j^{lin}$, $\mathbf{V}^{RB}$), we focus on the r-th entries of these vectors, defined respectively as (V_r^{meas}, $V_{j,r}^{nl}$, $V_{j,r}^{lin}$, V_r^{RB}). For notational simplicity, we will omit the subscript r, but these non-bold quantities will be understood to come from the r-th point. Please refer to Eq. (11) and Fig. 3 for their definition and visualization.

$$V^{\text{meas}} = \mathbf{e}_r^T \mathbf{V}^{meas} \qquad V_j^{nl} = \mathbf{e}_r^T \mathbf{V}_j^{nl} \qquad V_j^{lin} = \mathbf{e}_r^T \mathbf{V}_j^{lin} \qquad V^{RB} = \mathbf{e}_r^T \mathbf{V}^{RB}, \tag{11}$$

where $\mathbf{e}_r$ is a standard unit vector with a one in the r-th entry and zeros elsewhere.

Before presenting the algorithm steps, we would like to introduce quantities v and $\tilde{\varphi}_j^{\text{vel}}$ defined in Eqs. (12) and (13), respectively. Explaining and understanding each step of the system identification process is easier when these two parameters are defined. The former quantity, v, is the magnitude of the velocity complex amplitude measured at a specific point of the structure. The latter one, $\tilde{\varphi}_j^{\text{vel}}$, is the phase of the nonlinear velocity complex amplitude.

$$v = \left\| V^{\text{meas}} \right\| \approx \left\| V_j^{nl} + V_j^{lin} + V^{RB} \right\| \tag{12}$$

$$\tilde{\varphi}_j^{\text{vel}} = \angle\left(V_j^{nl}\right) = \angle\left(V^{\text{meas}} - V_j^{lin} - V^{RB}\right) = \tan^{-1}\left(\frac{-2\tilde{\zeta}_j \tilde{\omega}_{0,j} \Omega}{\tilde{\omega}_{0,j}^2 - \Omega^2}\right) \tag{13}$$

An interesting dependency between the nonlinear natural frequency and effective damping ratio can be derived from Eq. (13). Namely, equation (13) can be brought to a quadratic form (14), which – as indicated in (15) – always has two real solutions. Hence, the nonlinear natural frequency $\tilde{\omega}_{0,j}$ can be expressed as a function of the nonlinear damping ratio $\tilde{\zeta}_j$, see Eq. (16).

$$\tilde{\omega}_{0,j}^2 + \frac{2\tilde{\zeta}_j \Omega}{\tan(\tilde{\varphi}_j^{\text{vel}})}\, \tilde{\omega}_{0,j} - \Omega^2 = 0 \tag{14}$$

$$\frac{4\tilde{\zeta}_j^2 \Omega^2}{\tan^2(\tilde{\varphi}_j^{\text{vel}})} + 4\Omega^2 > 0 \quad \forall_{\tilde{\zeta}_j, \Omega, \tilde{\varphi}_j^{\text{vel}}} \tag{15}$$

$$\tilde{\omega}_{0,j} = f(\tilde{\zeta}_j) = \left(\frac{-\tilde{\zeta}_j}{\tan(\tilde{\varphi}_j^{\text{vel}})} \pm \sqrt{\frac{\tilde{\zeta}_j^2}{\tan^2(\tilde{\varphi}_j^{\text{vel}})} + 1} \right) \Omega \tag{16}$$

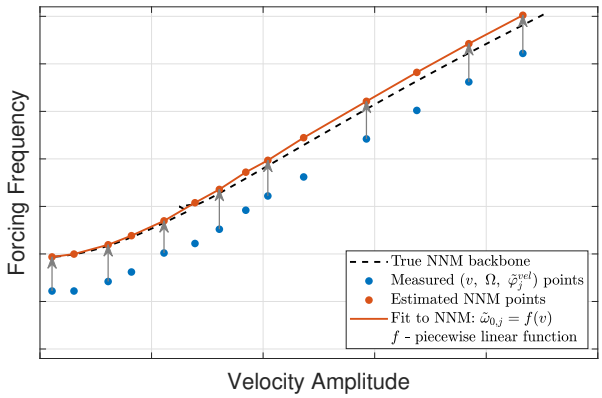

(a) Frequency vs. velocity amplitude

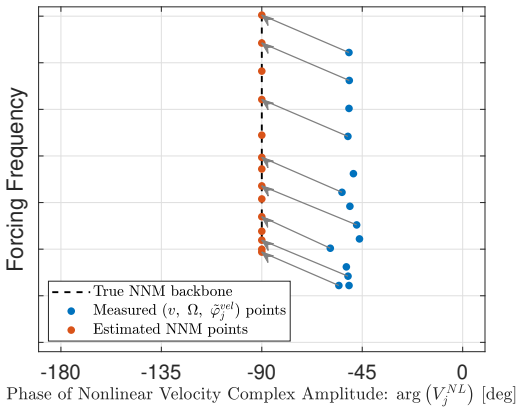

(b) Frequency vs. nonlinear velocity component phase

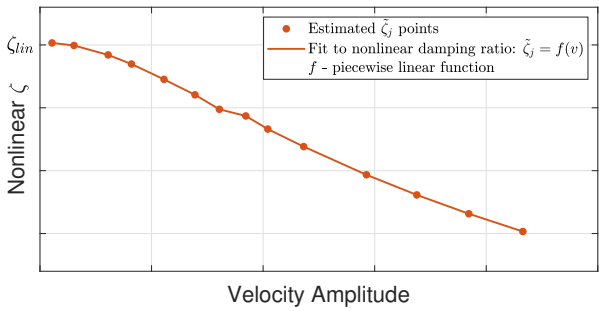

(c) Nonlinear damping ratio vs. velocity amplitude

Fig. 4: Visualization of the measured and estimated quantities in each algorithm step

To assure that the nonlinear eigen frequency is always a positive number one must detect which root in Eq. (16) is positive. It is trivial to prove that regardless of the lag or lead oscillation – $\tilde{\varphi}_j^{\text{vel}} \in (-180°, -90°)$ and $\tilde{\varphi}_j^{\text{vel}} \in (-90°, 0°)$, respectively – the positive value of $\tilde{\omega}_{0,j}$ is obtained at the root presented in Eq. (17).

$$\tilde{\omega}_{0,j} = f(\tilde{\zeta}_j) = \left(\frac{-\tilde{\zeta}_j}{\tan(\tilde{\varphi}_j^{\text{vel}})} + \sqrt{\frac{\tilde{\zeta}_j^2}{\tan^2(\tilde{\varphi}_j^{\text{vel}})} + 1} \right) \Omega \tag{17}$$

Hence, the formula presented in Eq. (17) can be used to model the nonlinear damping present in the system, and to the best of the authors knowledge, this expression has not been used previously to do so. This approach also proves very effective when it comes to the system identification process – as indicated in the case studies presented in this work.

2.2. System Identification Process

This section describes the system identification and outcomes validation processes. For clarity, the algorithm steps are additionally visualized in Fig. 4 and the proposed validation strategy is outlined in Fig. 5.

Algorithm Steps

The objective of the algorithm presented here is to estimate the Nonlinear Normal Mode backbone curve based on the *steady-state* data measured in its vicinity. The algorithm consists of three steps:

1. Measure the steady-state response of the system to a sinusoidal forcing at various force amplitudes, to obtain (v, Ω, $\tilde{\varphi}_j^{\text{vel}}$). These measured points are represented with blue dots in Fig. 4.

2. Use Eqs. (12) and (17) to assign $\tilde{\zeta}_j$ and $\tilde{\omega}_{0,j}$ values to every (v, Ω, $\tilde{\varphi}_j^{\text{vel}}$) triple (red dots).

3. Express $\tilde{\omega}_{0,j}$ and $\tilde{\zeta}_j$ as (e.g. piecewise linear) functions of the velocity magnitude v (red solid line).

A careful reader might ask how to extract $\tilde{\zeta}_j$ and $\tilde{\omega}_{0,j}$ parameters in the second step of the procedure presented above. Please note that expressions (12) and (17) form a system of two equations and two unknowns, as indicated in Eq. (18).

$$\begin{cases} v(\Omega;\ \tilde{\omega}_{0,j},\ \tilde{\zeta}_j) \approx \left\| V_j^{nl}(\Omega;\ \tilde{\omega}_{0,j},\ \tilde{\zeta}_j)\ +\ V_j^{lin}(\Omega)\ +\ V^{RB}(\Omega) \right\| \\ \tilde{\omega}_{0,j}(\Omega,\ \tilde{\varphi}_j^{\mathrm{vel}};\ \tilde{\zeta}_j) = \left(\frac{-\tilde{\zeta}_j}{\tan(\tilde{\varphi}_j^{\mathrm{vel}})} + \sqrt{\frac{\tilde{\zeta}_j^2}{\tan^2(\tilde{\varphi}_j^{\mathrm{vel}})} + 1} \right) \Omega \end{cases}, \tag{18}$$

where the expressions for V_j^{nl}, V^{lin} and V^{RB} are provided in Eqs. (11b,c,d) and (10b). The unknown parameters are $\tilde{\omega}_{0,j}$ and $\tilde{\zeta}_j$, while v, Ω and $\tilde{\varphi}_j^{\mathrm{vel}}$ are measured variables. Matrix $\mathbf{\Phi}$ and vector $\mathbf{F}$ from Eq. (10b) are measured and known, as well. The system of equations (18) can be solved e.g. with any iterative method.

After completing the three steps presented above, one obtains the nonlinear natural frequency expressed as a function of velocity magnitude: $\tilde{\omega}_{0,j} = \omega_{0,j}(v)$. It represents the estimate of the NNM backbone. Additionally, the algorithm approximates the shape of the function $\tilde{\zeta}_j = \zeta_j(v)$, which shows how the effective damping ratio changes with the vibration level.

Validation Steps

The results of the proposed algorithm can be validated in two ways, both of which will be used in this work. First, one could actually measure the NNM of the structure by tuning the phase of the nonlinear system to $-90°$. Then, the measured NNM curves could be compared with those found by the proposed approach (e.g. the red lines in Fig. 4), as shown in Fig. 5, where the point on the NNM found with the proposed method is shown with a ($\star$), while the one measured is shown with a purple square. (In practice one would not measure the latter because it would increase the time required to test, but in this work we do so in order to validate the approach.)

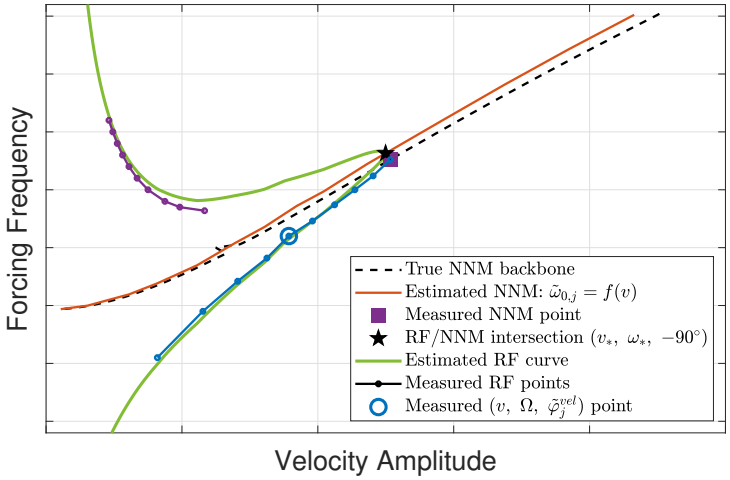

(a) Frequency vs. velocity amplitude

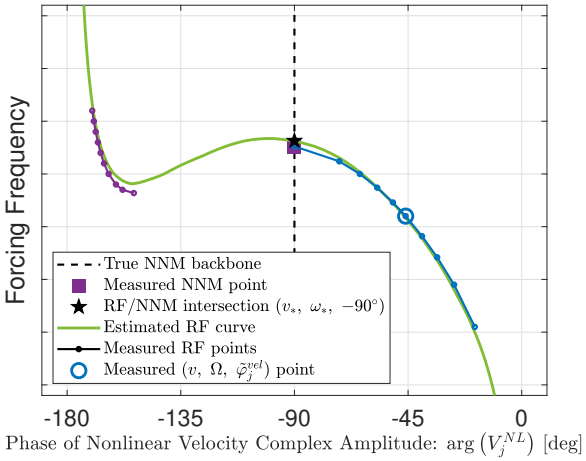

(b) Frequency vs. nonlinear velocity component phase

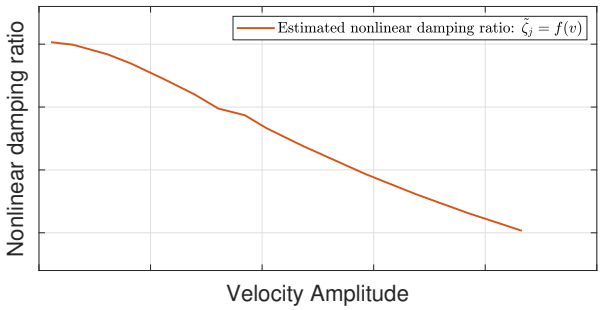

(c) Nonlinear damping ratio vs. velocity amplitude

Fig. 5: Visualization of the validation steps

Second, one could use the SNRM function to reconstruct the response function near the mode of interest and compare that to other non-resonant measurements, as shown by the curves in Fig. 5. One might find it interesting because it allows one to understand the extent to which the SNRM function can be used to model the system near resonance. To do so, one must first find the intersection between the response function and the NNM, denoted with (*), i.e. v_* and ω_* in Eq. (19), which is a simplified form of Eq. (12) for the case where the phase is $-90°$. Note that at the nonlinear resonance, the forcing frequency and nonlinear modal frequency must be equal: $\Omega = \tilde{\omega}_{0,j}(v_*) = \omega_*$. Equation (19) can be solved for v_* and ω_* with e.g. a derivative-free Picard-iteration (sometimes called a fixed-point iteration) algorithm.

$$v_* = \left\| \frac{\Phi_{j,r} \mathbf{\Phi}_j^T \mathbf{F}}{2i\tilde{\zeta}_j \omega_*}\ +\ V_{j,r}^{lin}(\omega_*)\ +\ V_r^{RB}(\omega_*) \right\| \tag{19}$$

Once the point at the resonance is known (i.e. the point marked with a ($\star$) in Fig. 5, Equation (10) can be used to estimate the lag (upper) and lead (lower) branches of the Response Functions using the (v_*, ω_*, $-90°$) triple as a start point. A similar technique was presented in [30]. As shown in the cases presented subsequently, the SNRM function was often found to perform quite well over a wide range of forcing frequency.

It is also interesting to highlight one additional point at this juncture. In terms of frequency (e.g. Fig. 4a), the measurements of the steady-state response (blue dots) are often quite close to the estimated NNM points (red dots). Considering Fig. 5, one can see that this occurs because the response function is quite narrow near the resonance if the system is lightly damped. However, in terms of phase these points (blue dots) are actually quite distant from the resonance (e.g. see Fig. 4b). This is further illustrated in Fig. 5a-b, where a typical measurement point, at about $-45°$ phase, is shown with an open blue circle. Hence, to actually measure the response at the NNM one would have to tune the forcing frequency quite a bit (assuming forcing amplitude is kept constant). Furthermore, one can see that the measurement is quite far from the NNM, and the point where the response is most likely to fall off of resonance, even though the corrections illustrated in Fig. 4a seem small.

In the next two sections the outcomes from four case studies are presented. The algorithm is first evaluated numerically using reduced order models of flat and curved clamped-clamped beams. Then the method is employed experimentally to identify the first NNMs of two 3D printed beams.

3. Numerical Investigation

3.1. Flat Clamped-Clamped Beam

The algorithm is first evaluated with data generated numerically using the traditional phase tuning (PT) approach. The test is performed on a *flat* beam with clamped-clamped boundary conditions. The beam is similar to the one studied in [43]. Its dimensions and mechanical properties are summarized in Tab. 1, while the parameters describing the underlying linear system are displayed in Tab. 2.

Tab. 1: Dimensions and mechanical properties of the numerical flat clamped-clamped beam.

Length [mm]	Width [mm]	Thickness [mm]	Young's modulus [GPa]	Density [$\frac{\text{kg}}{\text{m}^3}$]	Shear modulus [GPa]
228.6	12.7	0.787	204.8	7870	80.0

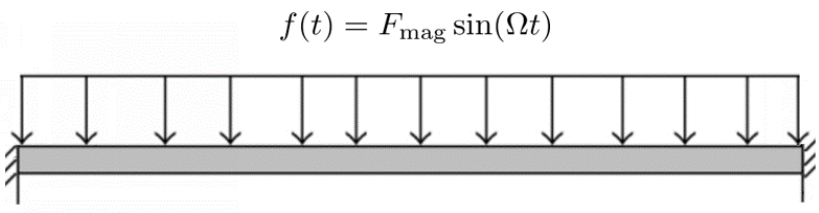

Fig. 6: Numerical model of a flat beam excited with a uniformly distributed sinusoidal force.

The structure, modeled with 40 beam elements resulting in a total of 246 DOFs, is used to generate the 4-mode ICE-ROM including the first four symmetric modes, i.e. modes 1, 3, 5 and 7. It is subjected to a uniformly distributed sinusoidal force (Fig. 6) representing a base excitation. The data points (v, Ω, $\tilde{\varphi}_j^{\text{vel}}$) are collected near the *first* Nonlinear Normal Mode.

To be complete, we should also provide the nonlinear equations of motion expressed in the modal domain. However – if the ICE-ROM of a beam consists of 4 modes, then its nonlinear part contains up to 30 polynomial terms per mode, and so it is relegated to Appendix A.

Tab. 2: Linear modal properties of the numerical flat beam. Modal damping ratio values are assigned manually.

Mode ID	1	3	5	7
$\omega_{0,k}$ [Hz]	79.02	427.46	1057.30	1970.70
ζ_k	0.05	0.0009	0.0008	0.0006

Figure 7 shows the collected (v, Ω, $\tilde{\varphi}_j^{\text{vel}}$) triples (measured at the beam's center) as well as the corresponding estimates of the NNM points. The data were collected by increasing the amplitude of the forcing and manually adjusting the frequency to keep the steady-state response near but not exactly at resonance, as determined by monitoring the shape of the Lisajous figure

(as shown in Fig. 2). The NNM Appropriation Indicator (NNMAI) was also computed for each point, and their values are between 0.5 and 0.7. This indicator, which was first proposed in [28], is a convenient tool to estimate how close the structure is to its nonlinear resonance. It requires decomposition of the response and forcing signals into user-specified harmonics via least square fitting of a multi-sine model function. Then, instead of trying to match their phases – which is tedious and often unsuccessful – the complex amplitudes, $\mathbf{X}_k$, are used in calculating the value of NNMAI defined in Eq. (20).

$$\Delta_{NNM} = \frac{1}{N_h} \sum_{k=1}^{N_h} \frac{\mathrm{Re}\{\mathbf{X}_k\}^T \mathrm{Re}\{\mathbf{X}_k\}}{\mathbf{X}_k^H \mathbf{X}_k}, \tag{20}$$

where N_h is the number of harmonics specified, $\mathbf{X}_k$ is the response complex amplitude of the k-th harmonic (computed with respect to the excitation complex amplitude and assuming that it is purely imaginary, as indicted in [28]) and $\Delta_{NNM} = 1$ when the system is at its nonlinear resonance.

The linear counterpart of the NNMAI is the well-know Mode Indicator Function (MIF) [44, 45], which is defined in in Eq. (21). The MIF can be used in determining how close the mono-harmonic response of the oscillating system $\mathbf{x}(t) = \mathrm{Re}\{\mathbf{X}e^{i\Omega t}\}$ is to its Linear Normal Mode.

$$\Delta_{lin} = \frac{\mathrm{Re}\{\mathbf{X}\}^T \mathrm{Re}\{\mathbf{X}\}}{\mathbf{X}^H \mathbf{X}}, \tag{21}$$

where $\mathbf{X}$ is the complex amplitude of the system's response computed with respect to the excitation complex amplitude. Additionally, the forcing complex amplitude is assumed to be purely imaginary.

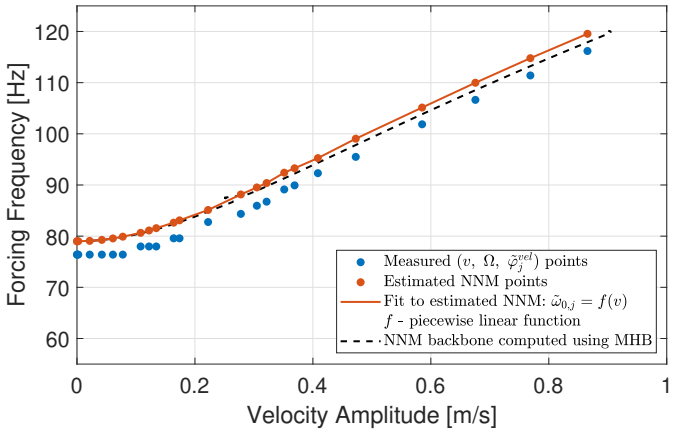

(a)

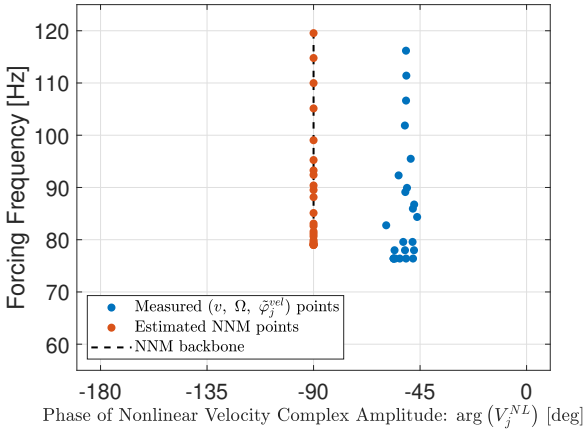

(b)

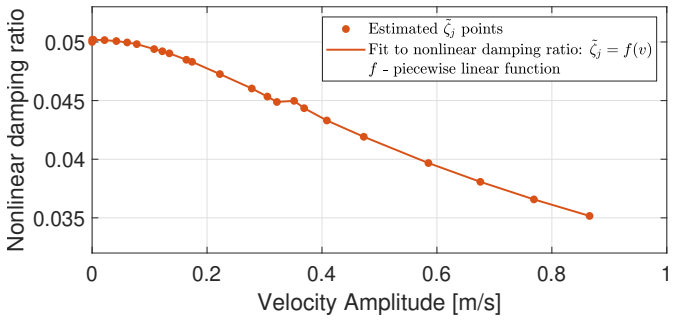

(c)

Fig. 7: Data measured and estimated resonant points. Case study with a numerical flat clamped–clamped beam model.

Since the algorithm is evaluated numerically, we have a benefit of finding the true Nonlinear Normal Mode curve using another and well-established algorithm. The NNM curve, computed by the Multi-Harmonic Balance (MHB) method [46, 47, 48, 49, 50, 51] using the first nine harmonics, is marked on charts with a dashed black line showing that the algorithm proposed here estimates the true NNM backbone with a satisfactory precision.

To further validate the system identification outcomes, the steady-state Response Functions estimated using Eq. 10 are compared to those measured numerically. Figure 8 presents four of such comparisons obtained for different forcing magnitudes: 2.669×10^{-3}, 4.448×10^{-3}, 8.896×10^{-3}, and 1.334×10^{-2} Newtons. The points and curves shown on the charts match each other. In this comparison the magnitudes of the linear terms in Eq. 10 were at least 200 times smaller than the nonlinear terms, and so they could have been neglected. There are some small discrepancies between the SNRM approximation and the true response, but the SNRM approach proposed here gives an excellent estimate and the ability to predict other forced responses from a few measured ones could prove very useful in practice.

Besides finding an estimate of the NNM backbone, the algorithm also returns the nonlinear damping ratio expressed as a function of velocity, see Fig.7c. In this particular example, where the system exhibits stiffening, $\tilde{\zeta}_j = \zeta_j(v)$ is found as a decreasing function of the motion amplitude. This result was expected, since the damping distribution in the numerical beam is modeled as vibration-level-independent (matrix $\mathbf{C}$ is constant).

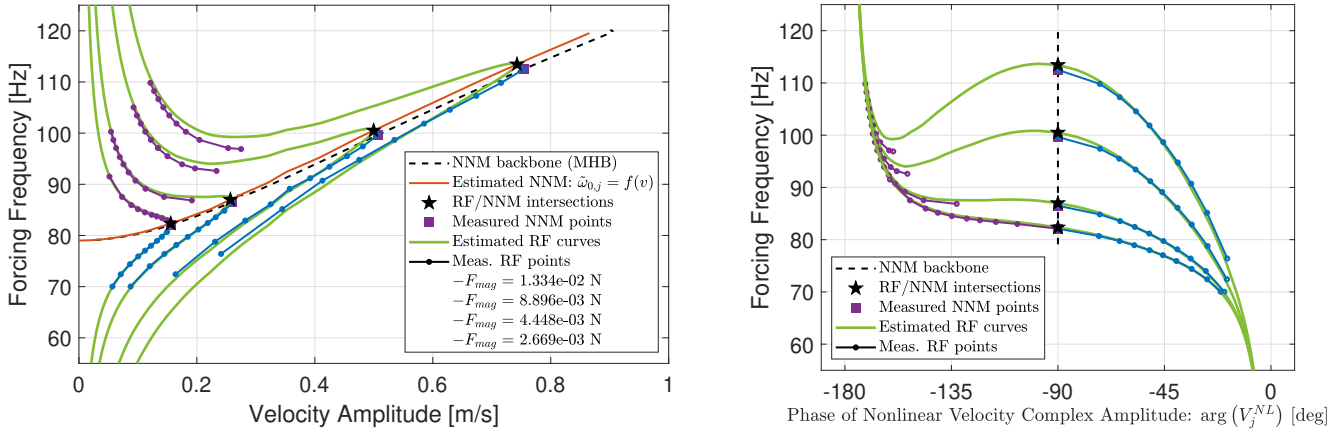

(a) **(b)**

Fig. 8: System ID validation: estimated vs. measured resonant points and Response Functions. Case study with a numerical flat clamped–clamped beam model.

3.2. Curved Clamped-Clamped Beam

The case study presented here is similar to the one from the previous section. This time, however, the numerical test involves a *curved* clamped–clamped beam that exhibits both softening and stiffening response due to the geometric nonlinearity. Table 3 shows the geometrical/mechanical properties of the beam.

Tab. 3: Dimensions and mechanical properties of the numerical curved clamped-clamped beam.

Length [mm]	Width [mm]	Thickness [mm]	Radius of curvature [m]	Young's modulus [GPa]	Density $[\frac{\text{kg}}{\text{m}^3}]$	Poisson's Ratio
304.8	12.7	0.508	11.43	204	7860	0.29

The beam is modeled with 400 shell elements resulting in a total of 3030 DOFs and it is excited with a uniformly distributed sinusoidal force (Fig. 9). The test is performed in the vicinity of the first NNM using a one-mode ICE-ROM (1st mode) to represent dynamics of the structure. The modal equation of motion is presented in (22), while the linear and nonlinear coefficients are defined in Tab. 4.

$$\ddot{q}_1 + 2\zeta_1\omega_{0,1}\dot{q}_1 + \omega_{0,1}^2 q_1 + \alpha_{11}q_1^2 + \beta_{111}q_1^3 = \mathbf{\Phi}_1^T\mathbf{f}(t) \tag{22}$$

Tab. 4: Linear and nonlinear modal properties of the numerical curved beam. The modal damping ratio value is assigned manually.

quantity	$\omega_{0,1}$ [Hz]	ζ_1	α_{11} $\left[\frac{1}{\sqrt{\text{kg}}\ \text{m}^{3/2}\ \text{s}^2}\right]$	β_{111} $\left[\frac{1}{\text{kg}\ \text{m}^2\ \text{s}^2}\right]$
value	64.78	0.05	-3.4380×10^9	6.2183×10^{12}

Similarly to the previous section, Figure 10 presents the measured steady–state inputs and the system identification outcomes. The Nonlinear Normal Mode Appropriation Indicator values of the data collected range from 0.7842 to 1.0. It is worth noting that most of the measured points have their NNMAI value closer to the lower bound of this set, as indicated in Fig. 10b. A few of (v, Ω, $\tilde{\varphi}_j^{\text{vel}}$) triples (collected at the beam's center) had to be measured very close of the nonlinear resonance. This was necessary because – in a case of systems exhibiting softening-stiffening characteristic – the near-resonant stability region switches from the lag (softening region) to lead (stiffening) side of the NNM backbone at a certain vibration amplitude. The transfer point between these stable lead-lag sides is naturally the backbone's point of minimum frequency. This is the reason why we needed to carefully approach and cross the nonlinear resonance at this minimum point in order to stay in the stable region.

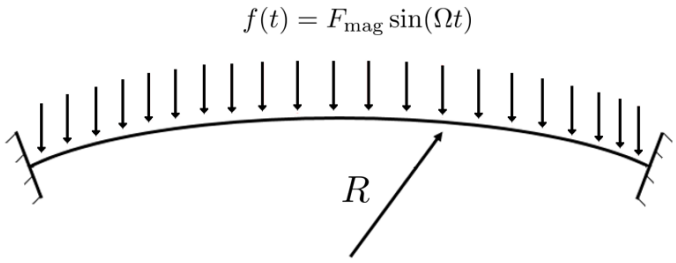

Fig. 9: The numerical model of a curved beam subjected to a uniformly distributed sinusoidal force.

Figures 11a-f illustrate the validation of the system ID outcomes. The estimated and true NNM curves match, as well as the estimated Response Functions and those measured with the numerical phase tuning approach. The RFs presented there correspond to three different forcing magnitudes, namely: 1.334×10^{-4}, 6.672×10^{-4} and 1.779×10^{-3} Newtons.

The model function of the nonlinear damping ratio $\tilde{\zeta}_1 = \zeta_1(v)$, presented in Fig. 10c, behaves contrarily and complementary to the the nonlinear modal frequency $\tilde{\omega}_{0,1}$. Namely, the effective damping ratio increases (decreases) when the system exhibits softening (stiffening). Additionally, a relatively sharp spike occurs in the $\tilde{\zeta}_1$-characteristic when the frequency becomes minimum.

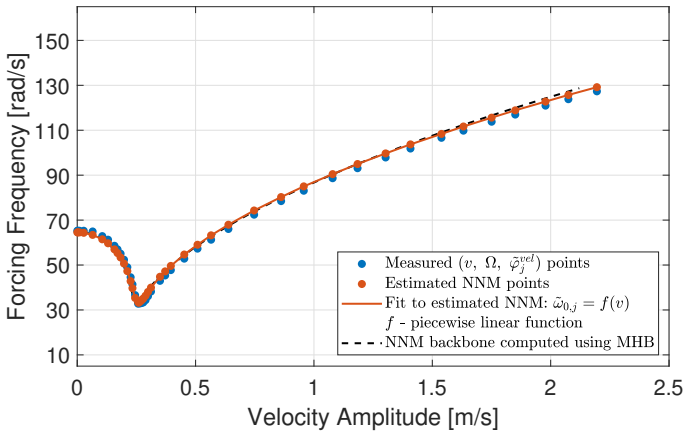

(a)

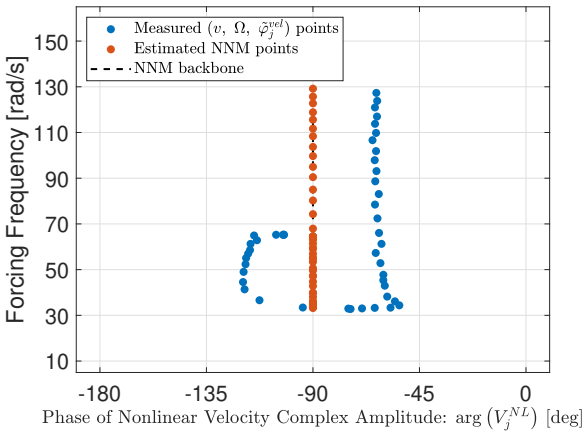

(b)

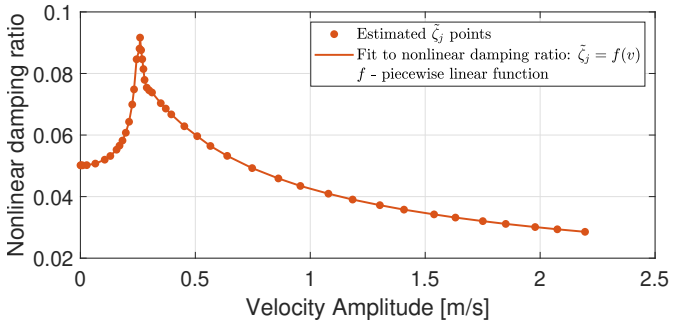

(c)

Fig. 10: Data measured and estimated resonant points. Case study with a numerical curved CC beam model.

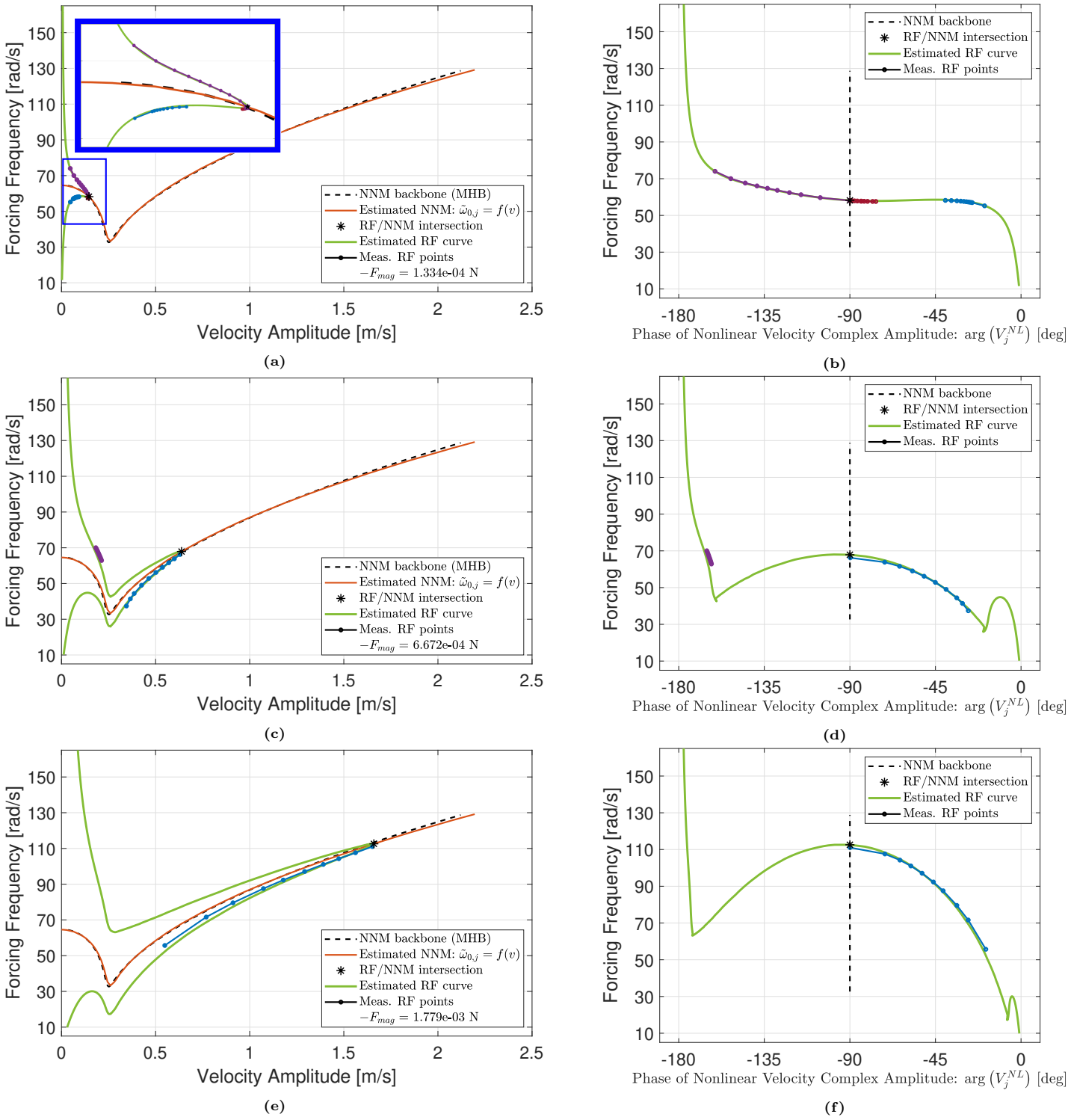

Fig. 11: System ID validation: estimated vs. measured resonant points and Response Functions. Case study with a numerical curved CC beam model.

4. Experimental Application to 3D–Printed Beams

The experimental set-up considered here is shown in Fig. 12. The structure is excited using a Modal Exciter 100 lbf Model 2100E11 powered by a 2050E05 Linear Power Amplifier. The control system (created using LabView) allows for changing the amplitude and frequency of the force applied to the structure with the voltage signal sent to the shaker [52, 53, 54]. The force applied is measured with a PCB208C04 load cell connected to a 3-channel Battery-powered ICP® Sensor Signal Conditioner Model 480B21. The oscillations of the beam's center point are measured with PSV-400 Scanning Vibrometer. Specifically, the phase between the force applied and velocity measured is monitored in real time to determine how far the structure is from its nonlinear resonance.

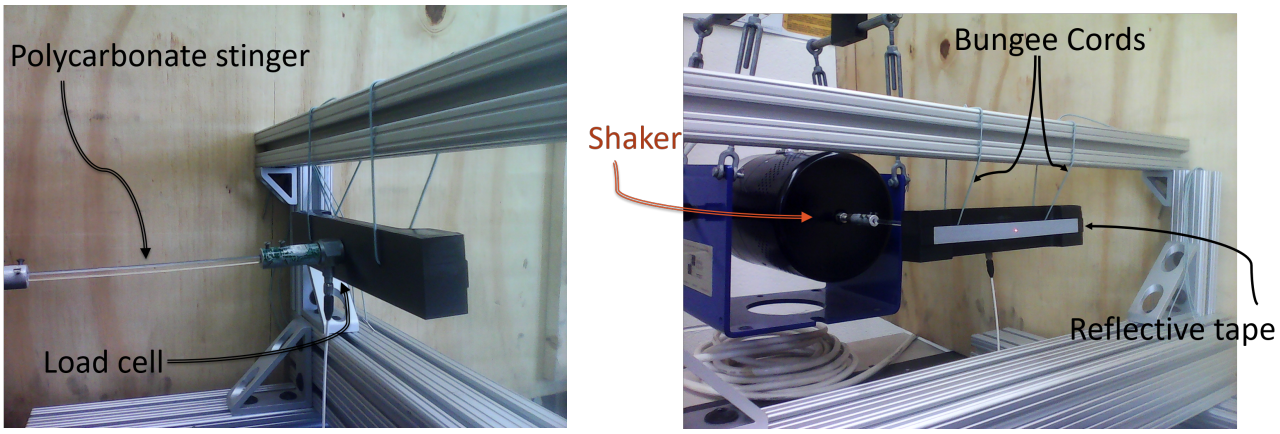

(a) **(b)**

Fig. 12: Photographs of the experimental setup: **(a)** back view; **(b)** front view.

Figure 13 shows the 3D–printed polylactide (PLA) samples used in the experiments. The thin and thick parts of the sample, called respectively beam and backing, are 3D–printed together and are non-detachable from one another. Such beam–backing connection prevents beam's ends from slipping even when it oscillates at high amplitudes, which is an often-encountered problem when the ends of a beam are tightened using bolted joints. On the other hand, eliminating the frictional nonlinearity from the system might narrow the application of the algorithm presented. The authors are aware that the identification of the bolted structures finds applications in many various branches of industry. However, the main goal of this article is to introduce this new SNRM-based technique and an attempt of employing the algorithm in system ID of a bolted structure will be a subject of the authors' future work.

The approximated mass and nominal dimensions common to all the 3D–printed samples are summarized in Table 5. The beams tested differ from one another with the radius of curvature, the values for which are specified in the sections below. It is worth noting that the beams' length and curvatures are nominal and subjected to very slight variation due to the 3D printing process. Their mechanical properties, such as Young's modulus or Poisson ratio, may also be difficult to determine for the same reason. Instead of measuring these quantities, we define the dynamic properties of each sample with their linear modal parameters, see e.g. Tab. 6 and Fig. 16.

Tab. 5: Nominal dimensions and mechanical properties common to all the 3D printed samples.

	Length [mm]	Width [mm]	Thickness [mm]	Approx. mass [g]
Beam	180	8	2	3.7696
Backing	200	30	30	130.00

The polycarbonate stinger connects the sample to the shaker. Moreover, the samples are designed such that the backing part can be modeled as a rigid body. This allows for converting the external point–force, applied via the stinger to the backing's center, into a *uniformly distributed* force acting on the beam, see Fig. 14. The geometry of the beam is represented with a rectangular grid of 44 points. In the tests performed, a LabView system [54] is used to bring the thin beam to the near-resonant oscillations and then its full-field dynamic response is measured over a several cycles using the Polytec software.

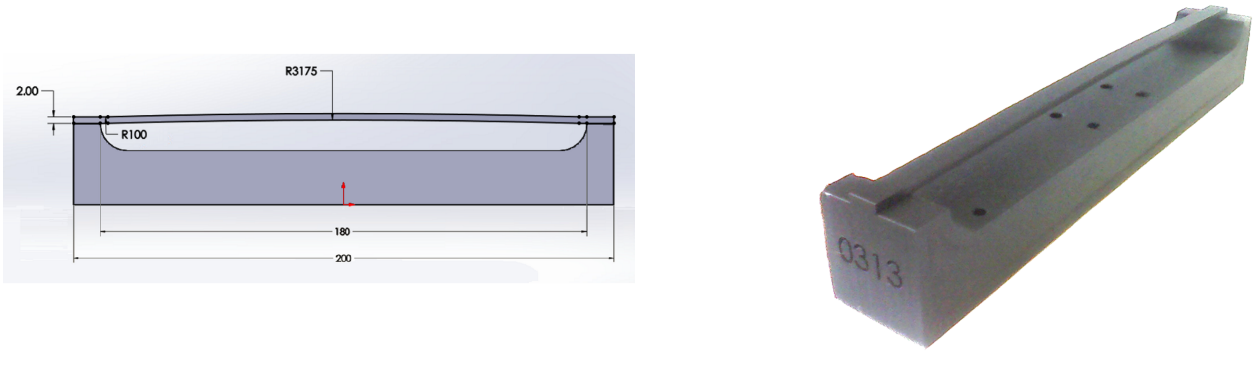

(a) (b)

Fig. 13: **(a)** Longitudinal cross-section of the SolidWorks [55] model of the curved beam and **(b)** photograph of one of the 3D–printed samples.

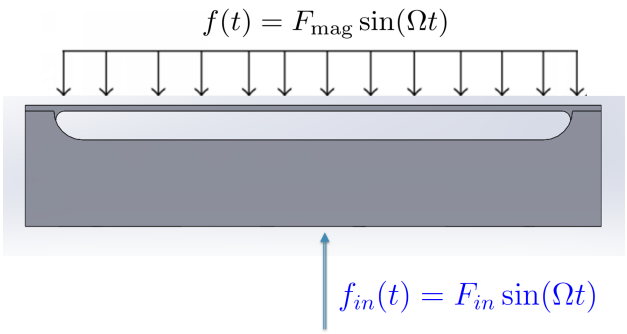

Fig. 14: The external point-force applied at the backing's center is converted into the force distribution acting on the beam.

4.1. Voltage into Distributed Force Conversion

In this subsection, the conversion between the point force signal applied at the backing into the distributed forcing acting on the beam is explained. This conversion is estimated via comparing the theoretical and measured low-amplitude Response Functions. As presented in Figs. 15a-b, three and five low level RFs are measured for, respectively, the curved and flat beams used in the case studies presented later in this article.

The low-amplitude Response Functions are measured on the curved beam for input voltage $F_{in} \in \{0.01, 0.02, 0.03\}$ volts, see Fig. 15a. The corresponding theoretical linear Response Functions – computed with Eq. (23) – are obtained for $F_{mag} \in \{1.9138, 4.6678, 7.3752\} \times 10^{-4}$ newtons. The F_{mag} data expressed as a function of F_{in} is presented in Fig. 15c together with the linear regression fit showing that $F_{mag} \approx 2.730673 \times 10^{-2} F_{in} - 8.090884 \times 10^{-5}$ – where F_{mag} and F_{in} are expressed in newtons and volts, respectively. It is worth noting that Figs. 15a-b show that the samples exhibits a slight frequency shift even when the oscillations are low-level. However, the authors still decided to use Eq. (23) (with parameter $\omega_{0,1}$ adjusted accordingly) to estimate the voltage-force conversion.

$$\mathbf{V}_{lin}^{theory} = \sum_{k=1}^{N_{RB}} \frac{-\mathbf{\Phi}_k^{RB} \left(\mathbf{\Phi}_k^{RB}\right)^T \mathbf{F}}{\Omega} + \sum_{k=1}^{N_{lin}} \frac{\mathbf{\Phi}_k \mathbf{\Phi}_k^T \mathbf{F} \Omega}{\omega_{0,k}^2 - \Omega^2 + 2i\zeta_k \omega_{0,k} \Omega} \tag{23}$$

The conversion for the flat beam is obtained with analogical steps. Five low-level Response Functions are measured and modeled for, respectively: $F_{in} \in \{0.02, 0.03, 0.04, 0.05, 0.06\}$ volts and $F_{mag} \in \{2.5507, 4.5867, 6.6454, 8.5029, 10.8047\} \times 10^{-4}$ newtons, as presented in Fig. 15b. F_{mag} is depicted as a function of F_{in} in Fig. 15d showing that $F_{mag} \approx 2.042420 \times 10^{-2} F_{in} - 1.551595 \times 10^{-4}$. The F_{mag} and F_{in} quantities are again expressed in newtons and volts, respectively

4.2. Identification of Curved and Flat Beams

To verify the results obtained in the numerical study, the identification process is now performed on 3D-printed curved and flat beams. The nominal geometric dimensions of the samples are summarized in Tab. 5 and the radius of curvature of the curved beam is 3175 mm.

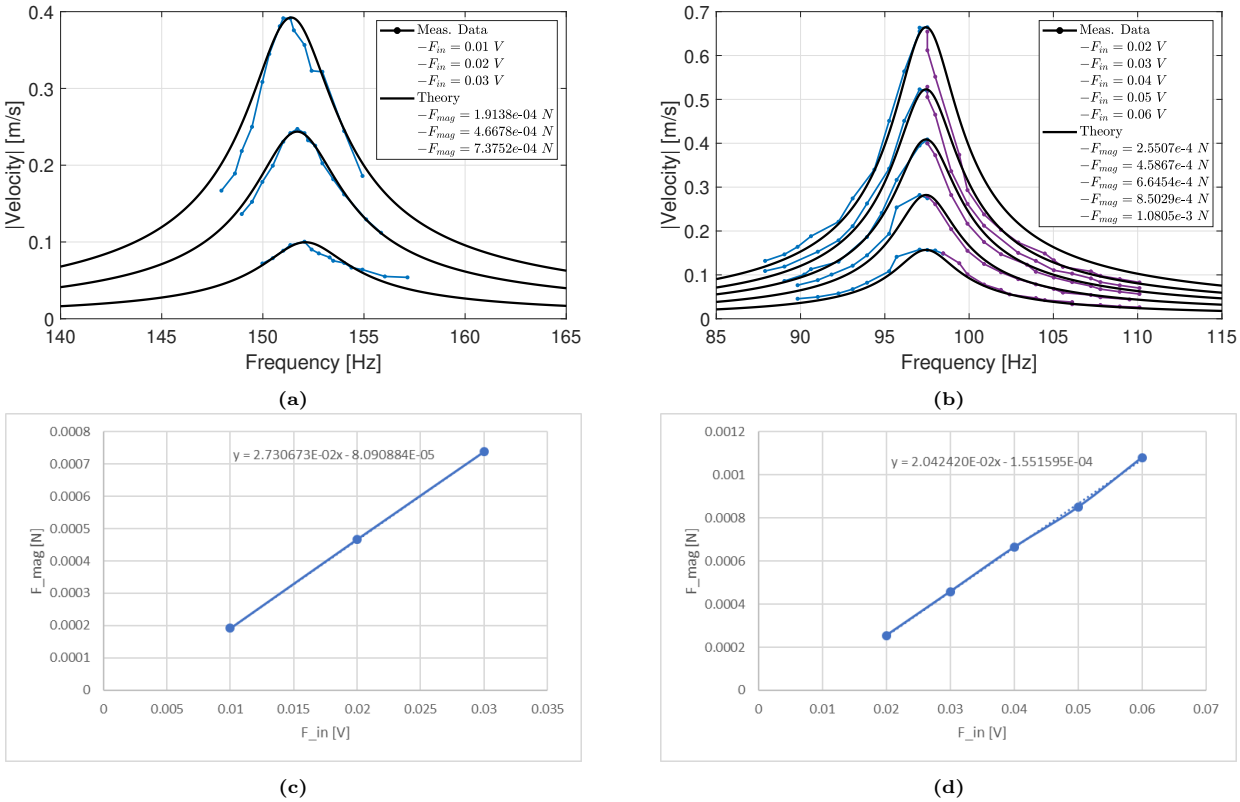

Fig. 15: Comparison of the low-level response functions measured and modeled in the vicinity of linear mode 1 using, respectively: **(a)** curved and **(b)** flat 3D-printed beams. Subplots **(c)** and **(d)** show the linear regression fits to functions $F_{mag} = F_{mag}(F_{in})$ corresponding to the data presented in subplots **(a)** and **(b)**, respectively.

The linear modal properties of the beams are measured in the low-amplitude vibration tests. The Frequency Response Functions and parameters describing their underlying linear systems are presented in Fig. 16 and Tab. 6, respectively. The dynamics of the beams is represented with modes 1 and 3 (first two symmetric modes) which, as indicated in Fig. 16, are well-separated.

Tab. 6: Linear modal properties of the 3D-printed curved and flat beams.

	Curved Beam		Flat Beam	
Mode ID	1	3	1	3
$\omega_{0,k}$ [Hz]	153.2144	592.6020	97.4457	534.9189
ζ_k	0.0138	0.0195	0.0189	0.0243

The steps taken to identify both curved and flat beams are very similar. First of all, phase-resonance testing is performed to collect the steady-state triples $(v,\ \Omega,\ \tilde{\varphi}_j^{\text{vel}})$ in the vicinity of the *first* nonlinear mode. They are visualized in Figs. 17 and 18 with blue dots and their NNM Appropriation Indicators range from 0.4914 to 0.9373 (in a case with curved beam) and from 0.6831 to 0.9052 (flat beam). The proposed inverse SNRM-based algorithm was then used to estimate the NNM near each of these points, and the estimated NNMs are shown with red dots. Similarly to the corresponding numerical case study, the curved and flat samples exhibit softening-stiffening and pure stiffening characteristics, respectively.

The validation of the results is presented in Figs. 19 and 20. The nonlinear resonant points and Response Functions are computed and compared to those collected experimentally for the same excitation levels. These quantities are measured on the curved beam for $F_{mag} \in \{1.279,\ 4.000,\ 6.719\}\times 10^{-3}$ Newtons, while in case of the flat sample $F_{mag} \in \{1.066,\ 2.287,\ 4.169\}\times 10^{-3}$ Newtons. As presented in the charts – they match when it comes to both frequency-amplitude and frequency-phase characteristics. However, it is worth noticing that Figs. 19e-f and 20e-f show that there is only a slight discrepancy between the lag (or upper) branches of the Response Functions when the excitation force is large.

This comparison illustrates that the inverse SNRM-based algorithm presented here allows for a successful system identification of a mechanical system experiencing softening-stiffening characteristic with a significant nonlinear frequency shift. In the case with curved beam, the eigen-frequency shift is approximately 25.71 Hz, which stands for a 16.78% change with respect

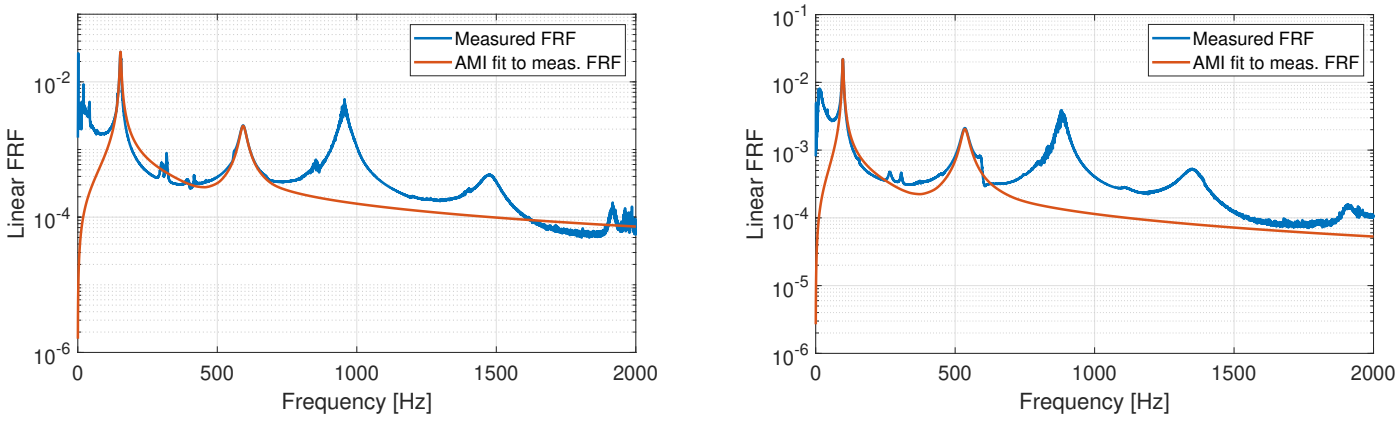

Fig. 16: Linear Frequency Response Function of the 3D-printed **(a)** curved and **(b)** flat beams. Fit to the FRFs computed using the Algorithm of Mode Isolation (AMI) [56].

to the linear natural frequency, $\omega_{0,1}$. The frequency shift exhibited by the flat beam is even more significant, it increases by approximately 35.79 Hz, a relative change of 37.16%.

The case study performed on e.g. the curved beam shows that with only 31 steady-state and near-resonant measurements (marked with blue dots in Fig. 17) we are able to reconstruct *any* frequency-amplitude-phase characteristic (see Fig. 19) in the amplitude range of interest. To give the reader a way to quantify it, we collected 85 steady-state points to measure *only one* nonlinear Response Function displayed in Figs. 19e-f. This shows how significant reduction of work and time spent on the phase tuning testing is allowed by the inverse SNRM-based technique presented here. It is also worth noticing that besides estimating the stable RF branches, the algorithm finds their unstable parts as well. These unstable branches can usually not be measure using the traditional Phase Resonance Testing approach (i.e. a controller would be needed to stabilize the system in order to measure them).

Another advantage of the inverse SNRM-based routine is that it allows one to estimate the NNM backbone without collecting the resonant points directly. They can be estimated based on the near-resonant measurements, speeding up the testing significantly. Indeed, when seeking to measure the nonlinear resonant point directly for the presented structures, we found that the system would often fall off the stable branch. Typically multiple attempts were needed to measure one NNM point in these cases, increasing the testing time. The algorithm proposed here allowed the backbone to be estimated without a necessity of approaching it too closely, hence this was not a problem except near the point of minimum frequency for the curved beam, where the NNM curve had to be crossed to remain in the stable region. In the case study presented in this section, collecting one steady-state measurement took between 10 and 20 seconds. Thus, the algorithm proposed here reduced the time spent in the laboratory from a couple of hours to just a few minutes. As a result, the structure was also exposed to significantly fewer cycles of vibration at high amplitudes, and was less likely to be damaged or develop fatigue fractures. In the early stages of this work several 3D printed beams were destroyed or developed fatigue cracks or delaminations after testing for too long or at too high of amplitudes.

A careful reader will notice that there is a slight inconsistency between the measured linear data presented in Tab. 6 and the estimated damping curves in Figs. 17c and 18c. Namely, in order to be considered as physically accurate, the nonlinear $\tilde{\zeta}_j$ curve should converge to the linear damping ratio value when the motion amplitude approaches zero. In the case study presented, it seems that the inverse SNRM-based algorithm estimates the damping ratio slightly incorrectly in the low vibration range. This discrepancy might be caused due to the basic assumption that the shape of the nonlinear normal mode is invariant of the response amplitude; however this requires more in-depth research and will be investigated by the authors in their future work. To evaluate how important that error might be, we reconstructed the Response Functions using the nonlinear damping curves before and after the manual adjustment. Figures 19 and 20 show that there is practically no difference between them. An additional discussion on how this manual modification impacts the modal viscous damping present in the system is provided in Appendix B.

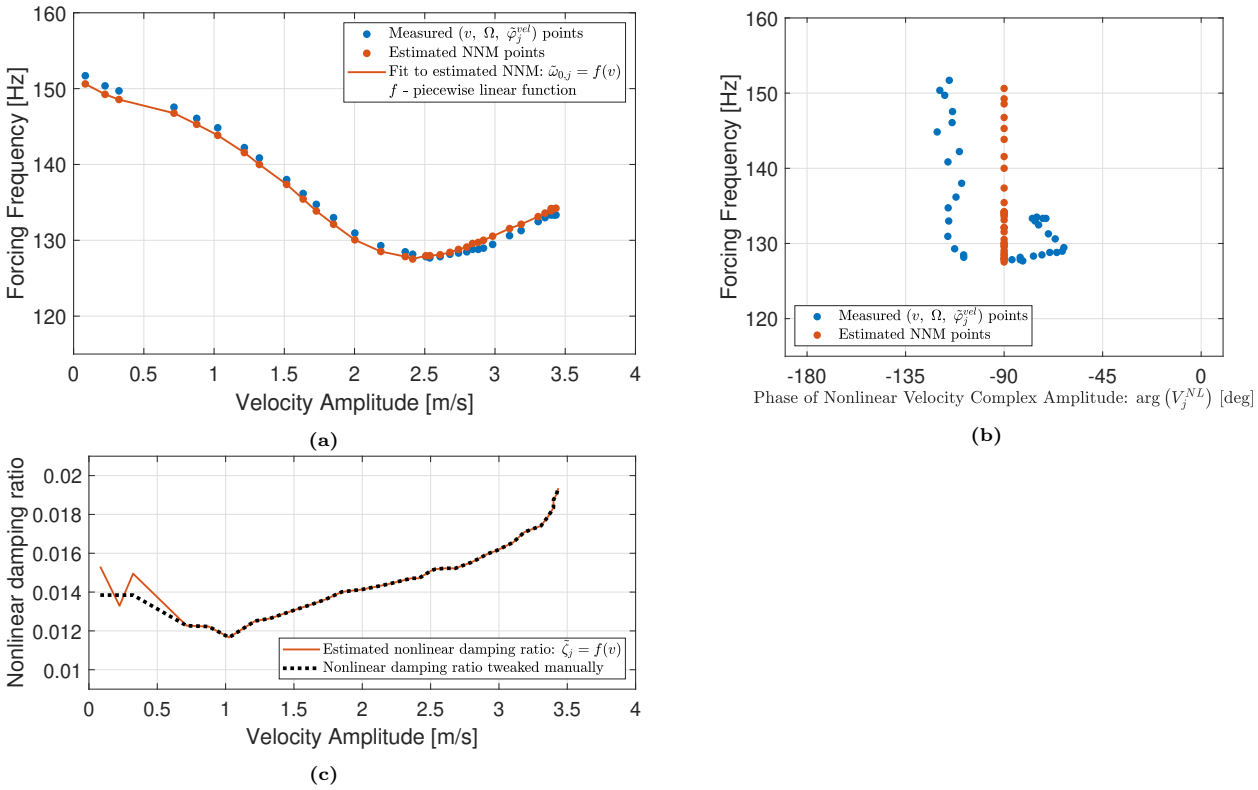

Fig. 17: Data measured and estimated resonant points. Case study with a 3D-printed curved beam.

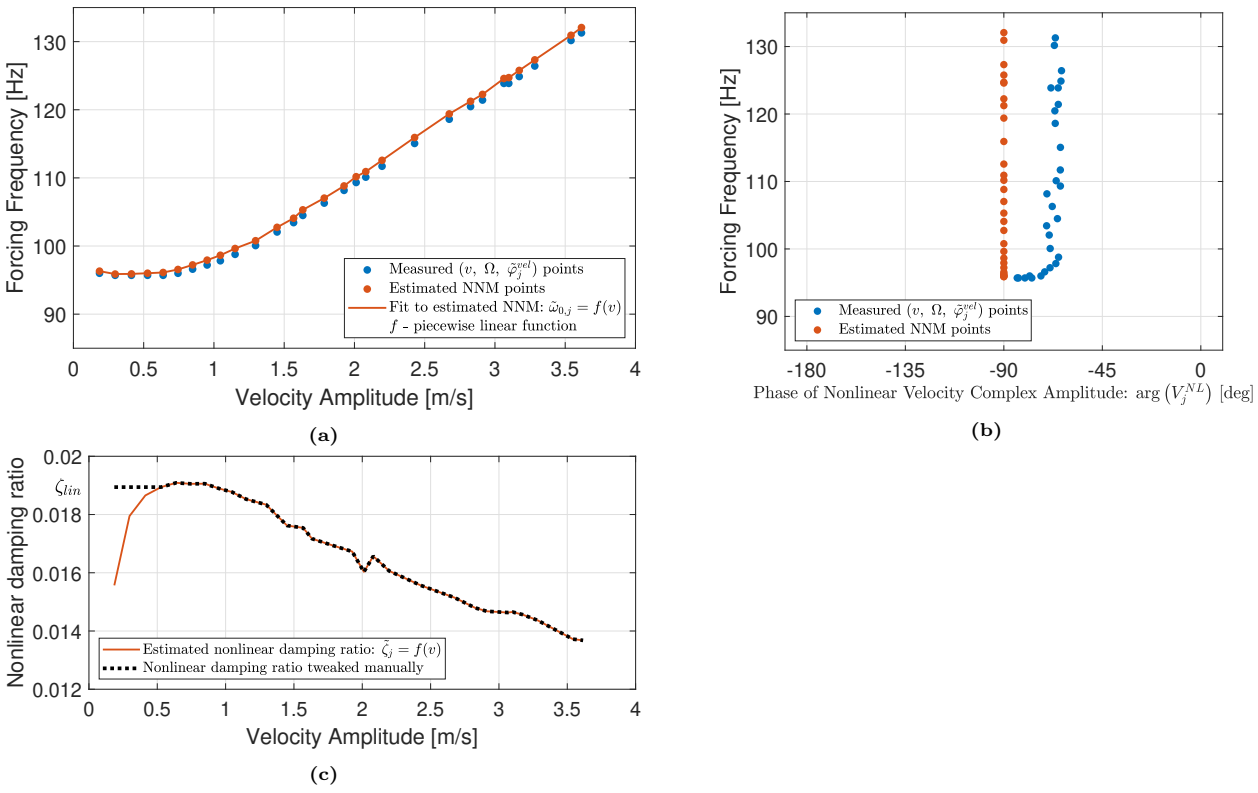

Fig. 18: Data measured and estimated resonant points. Case study with a 3D-printed flat beam.

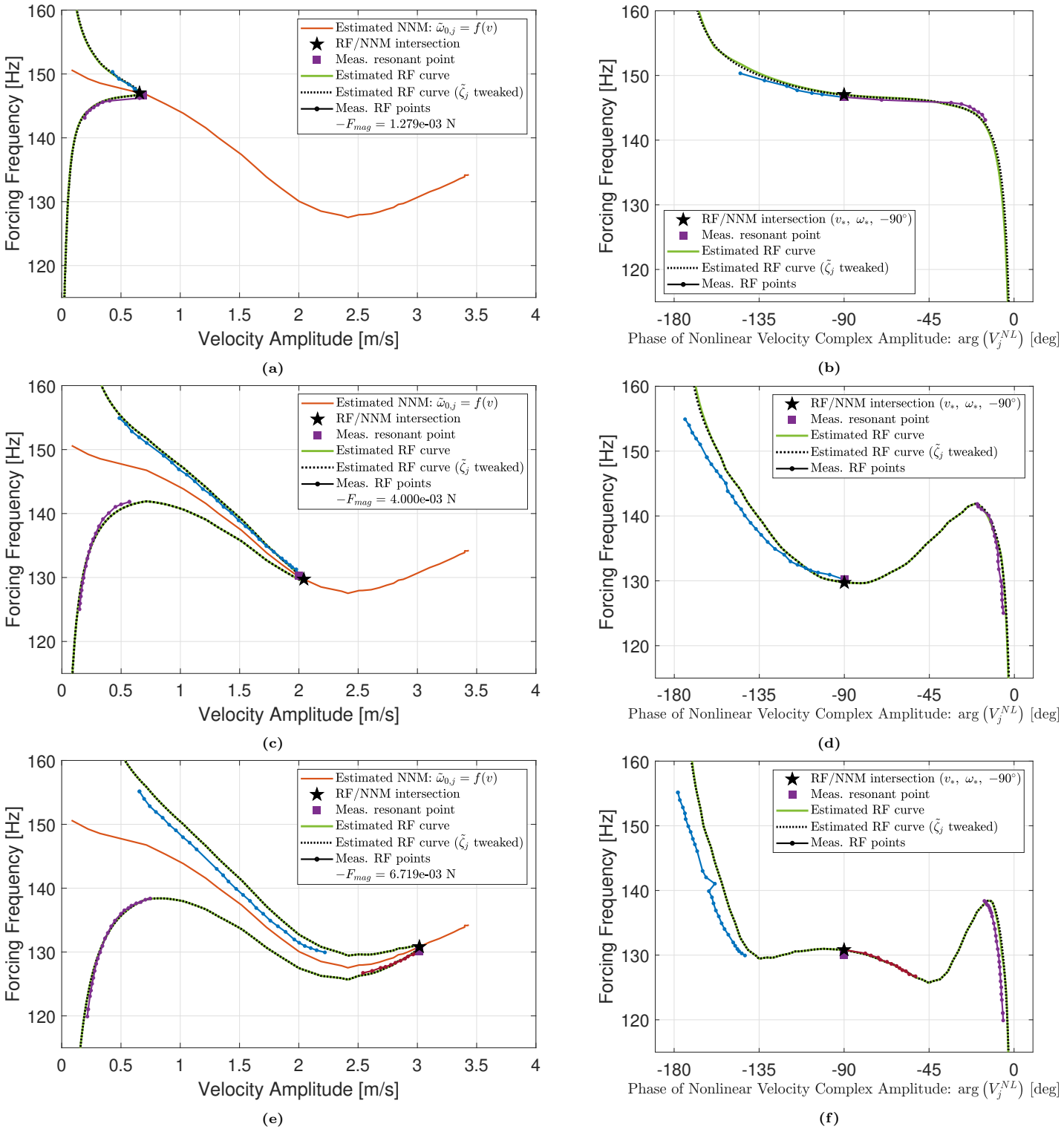

Fig. 19: System ID validation: estimated vs. measured resonant points and Response Functions. Case study with a 3D-printed curved beam.

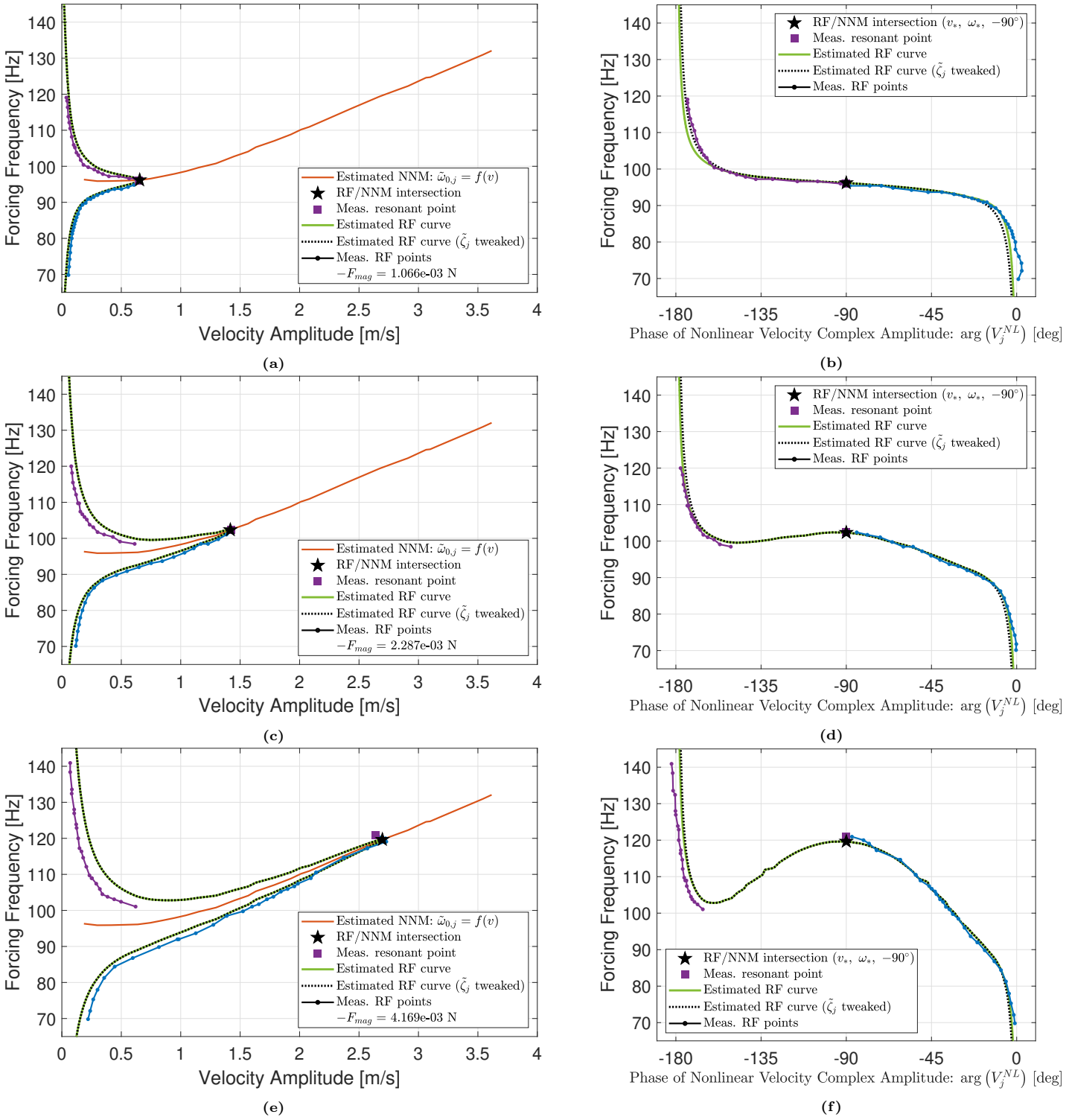

Fig. 20: System ID validation: estimated vs. measured resonant points and Response Functions. Case study with a 3D-printed flat beam.

5. Conclusions and Future Work

This work has presented a new system identification technique, which can be classified as a modal method. The algorithm can be successfully used in the system identification of structures with geometrical and/or physical nonlinearities. The technique proposed, called the inverse SNRM-based method, is based on the original SNRM formulation but utilizes it in a novel way. Namely, in order to estimate one point on the NNM curve it requires collecting *only one* steady-state and near-resonant measurement. Moreover, the algorithm does not need to be combined with any additional formulas to model the nonlinear damping present in the system. Instead, it utilizes an expression already contained in the original SNRM function.

In the case studies presented, the inverse SNRM-based algorithm successfully identified mechanical systems that exhibits stiffening and softening-stiffening characteristic, such as flat and curved beams, respectively. Moreover, the method managed to capture the significant eigen-frequency shifts of up to 35.79 Hz, which represents a change of 37.16% with respect to the linear natural frequency of the structure.

Since the algorithm estimates the Nonlinear Normal Mode backbone based on the near-resonant inputs, it can also be considered as safe (or nondestructive) to the tested structures. Keeping a distance from the nonlinear resonance allows additionally to minimize the issues with premature jump phenomenon, an often-encountered problem in the manual Phase Resonance Testing. Additionally, thanks to this new SNRM-based strategy the Phase Tuning testing becomes more time efficient. In order to find the NNM backbone, the measurements do not have to be taken precisely at the nonlinear resonances. Instead, they can be collected in the NNM's vicinity and provided to the inverse SNRM-based algorithm, which will then estimate the location of the backbone curve. Moreover, the algorithm can be used to estimate both the stable and unstable branches of the nonlinear Response Functions near the resonance.

The proposed approach is based on the Single Nonlinear Resonant Mode theory which limits the application of the algorithm to structures with well-separated modes and no internal resonance. Moreover, the method requires the accurate identification of linear modes in the low-amplitude vibration tests and it assumes that the shape of the nonlinear normal mode is invariant of the response amplitude.

Future works will employ this SNRM-based technique to identify more complex mechanical systems, such as structures with a friction nonlinearity. The application of the algorithm to the cases where the modes are not well-separated will also be investigated. Moreover, the authors have already taken an initial step towards extending the algorithm such that it could detect the presence of modal coupling and/or multi-harmonics in the system's response [57]. However, this modification – if at all feasible – requires more in-depth research.

Acknowledgments

This work was partially supported by the Air Force Office of Scientific Research, Award # FA9550-17-10009, under the Multi-Scale Structural Mechanics and Prognosis program managed by Dr. Jaimie Tiley. The authors would also like to thank Joseph Hollkamp from the Air Force Research Laboratory's Structural Sciences Center, for his insightful comments and suggesting several improvements to this work.

Appendix A. Modal EOM of the Numerical Flat Beam Model

This section presents the modal equation of motion of the flat beam from section 3.1. As presented in Eq. (A.1), the ICE-ROM is created using 4 modes (the first four symmetric modes) and the nonlinear part of each modal EOM consists of 30 polynomial terms. The linear and nonlinear coefficients values are defined in Tabs. 2 and A.1, respectively. Note that the subscripts of the parameters correspond to the product of terms they multiply, e.g.: β_{111} multiplies term q_1^3, while β_{123} – term $q_1 q_2 q_3$.

$$
\begin{aligned}
&\ddot{q}_1 + 2\zeta_1\omega_{0,1}\dot{q}_1 + \omega_{0,1}^2 q_1 + \alpha_{11}^1 q_1^2 + \alpha_{12}^1 q_1 q_2 + \cdots + \beta_{111}^1 q_1^3 + \beta_{112}^1 q_1^2 q_2 + \cdots = \mathbf{\Phi}_1^T \mathbf{f}(t) \\
&\ddot{q}_2 + 2\zeta_2\omega_{0,2}\dot{q}_2 + \omega_{0,2}^2 q_2 + \alpha_{11}^2 q_1^2 + \alpha_{12}^2 q_1 q_2 + \cdots + \beta_{111}^2 q_1^3 + \beta_{112}^2 q_1^2 q_2 + \cdots = \mathbf{\Phi}_2^T \mathbf{f}(t) \\
&\ddot{q}_3 + 2\zeta_3\omega_{0,3}\dot{q}_3 + \omega_{0,3}^2 q_3 + \alpha_{11}^3 q_1^2 + \alpha_{12}^3 q_1 q_2 + \cdots + \beta_{111}^3 q_1^3 + \beta_{112}^3 q_1^2 q_2 + \cdots = \mathbf{\Phi}_3^T \mathbf{f}(t) \\
&\underbrace{\ddot{q}_4 + 2\zeta_4\omega_{0,4}\dot{q}_4 + \omega_{0,4}^2 q_4}_{\text{linear part}} + \underbrace{\alpha_{11}^4 q_1^2 + \alpha_{12}^4 q_1 q_2 + \ldots}_{\text{quadratic stiffness part}} + \underbrace{\beta_{111}^4 q_1^3 + \beta_{112}^4 q_1^2 q_2 + \ldots}_{\text{cubic stiffness part}} = \mathbf{\Phi}_4^T \mathbf{f}(t)
\end{aligned}
\tag{A.1}
$$

Tab. A.1: Values of the polynomial coefficients from the nonlinear modal equation of motion of the flat beam. The reduced order model consists of modes 1, 3, 5 and 7.

Parameter \ Mode		1	3	5	7
α_{11}		1.858E+07	2.765E+06	-2.593E+06	4.293E+07
α_{22}		-2.454E+07	1.983E+07	-7.412E+06	1.037E+06
α_{33}		1.007E+06	3.689E+07	-1.271E+07	5.892E+06
α_{44}		2.685E+07	-2.182E+07	-5.087E+06	1.148E+07
α_{12}	$\left[\frac{1}{\sqrt{\text{kg}}\ \text{m}^{3/2}\ \text{s}^2}\right]$	5.530E+06	-4.908E+07	-6.979E+06	-5.048E+07
α_{13}		-5.185E+06	-6.979E+06	2.014E+06	-1.954E+07
α_{14}		8.585E+07	-5.048E+07	-1.954E+07	5.371E+07
α_{23}		-6.979E+06	-1.482E+07	7.377E+07	1.100E+07
α_{24}		-5.048E+07	2.075E+06	1.100E+07	-4.364E+07
α_{34}		-1.954E+07	1.100E+07	1.178E+07	-1.017E+07
β_{111}		1.375E+13	-1.107E+13	-8.587E+12	5.968E+12
β_{122}		-3.321E+13	1.268E+14	-1.281E+13	1.183E+13
β_{133}		-2.576E+13	-1.281E+13	3.053E+14	-2.231E+12
β_{144}		1.790E+13	1.183E+13	-2.231E+12	5.691E+14
β_{211}		1.268E+14	-2.670E+14	-2.341E+13	1.601E+13
β_{222}		-8.901E+13	8.956E+14	-2.180E+14	1.975E+14
β_{233}		-2.341E+13	-6.541E+14	2.487E+15	2.230E+14
β_{244}		1.601E+13	5.924E+14	2.230E+14	4.603E+15
β_{311}		3.053E+14	-2.073E+14	-5.593E+14	9.317E+13
β_{322}	$\left[\frac{1}{\text{kg}\ \text{m}^2\ \text{s}^2}\right]$	-2.073E+14	2.487E+15	-1.761E+15	3.681E+14
β_{333}		-1.864E+14	-5.868E+14	6.279E+15	8.698E+14
β_{344}		9.317E+13	3.681E+14	2.609E+15	1.217E+16
β_{411}		5.691E+14	-4.317E+14	-3.327E+14	8.486E+14
β_{422}		-4.317E+14	4.603E+15	-9.444E+14	3.119E+15
β_{433}		-3.327E+14	-9.444E+14	1.217E+16	5.109E+15
β_{444}		2.829E+14	1.040E+15	1.703E+15	2.267E+16
β_{133}		-2.561E+13	-4.682E+13	-4.147E+14	-1.226E+14
β_{144}		2.367E+13	3.202E+13	-1.226E+14	-8.634E+14
β_{144}		-4.462E+12	-1.226E+14	1.863E+14	-6.655E+14
β_{244}		-1.226E+14	4.460E+14	7.362E+14	-1.889E+15

Appendix B. Impact of the $\tilde{\zeta}_j$-curve Shape on the Validation Results

As mentioned in section 4.2 - the inverse SNRM-based algorithm seems to have estimated the nonlinear damping ratio incorrectly at very low oscillation amplitudes. To be more precise, the $\tilde{\zeta}_j$-curves obtained in the experimental case studies do not intersect their linear damping ratio values, which are found in separate linear experimental vibration analyses. Note that the numerical case studies presented in this work do not suffer from this issue. The solution we propose in section 4.2 is a manual adjustment of the damping functions such that they start from the linear values at low amplitudes, as illustrated in Figs. 17c and 18c. In this section, we would like to investigate how this manual modification impacts one physical quantity of the mechanical systems, namely the modal viscous damping.

According to the light damping approximation heuristic, the linear viscous damping of the k-th mode can be expressed as in Eq. (B.1).

$$\hat{C}_{kk} = \mathbf{\Phi}_k^T \mathbf{C} \mathbf{\Phi}_k \approx 2\omega_{0,k}\zeta_k \tag{B.1}$$

Since this work focuses on nonlinear structures, whose eigen-frequencies and damping ratios are vibration-level-dependent, we decided to investigate if and how this viscous damping changes with the motion amplitude. To do so, we would like to define a quantity called nonlinear modal damping, which is a product of the nonlinear frequency and effective damping ratio functions, see Eq. (B.2).

$$\tilde{\hat{C}}_{jj} = 2\tilde{\omega}_{0,j}\tilde{\zeta}_j \tag{B.2}$$

Figure B.1 summarizes how the nonlinear damping coefficient changes with the vibration amplitude in each of the four case studies described in this article. As illustrated in Fig. B.1a, the $\tilde{\hat{C}}_{11}$ of the numerical flat beam tends to stay constant.

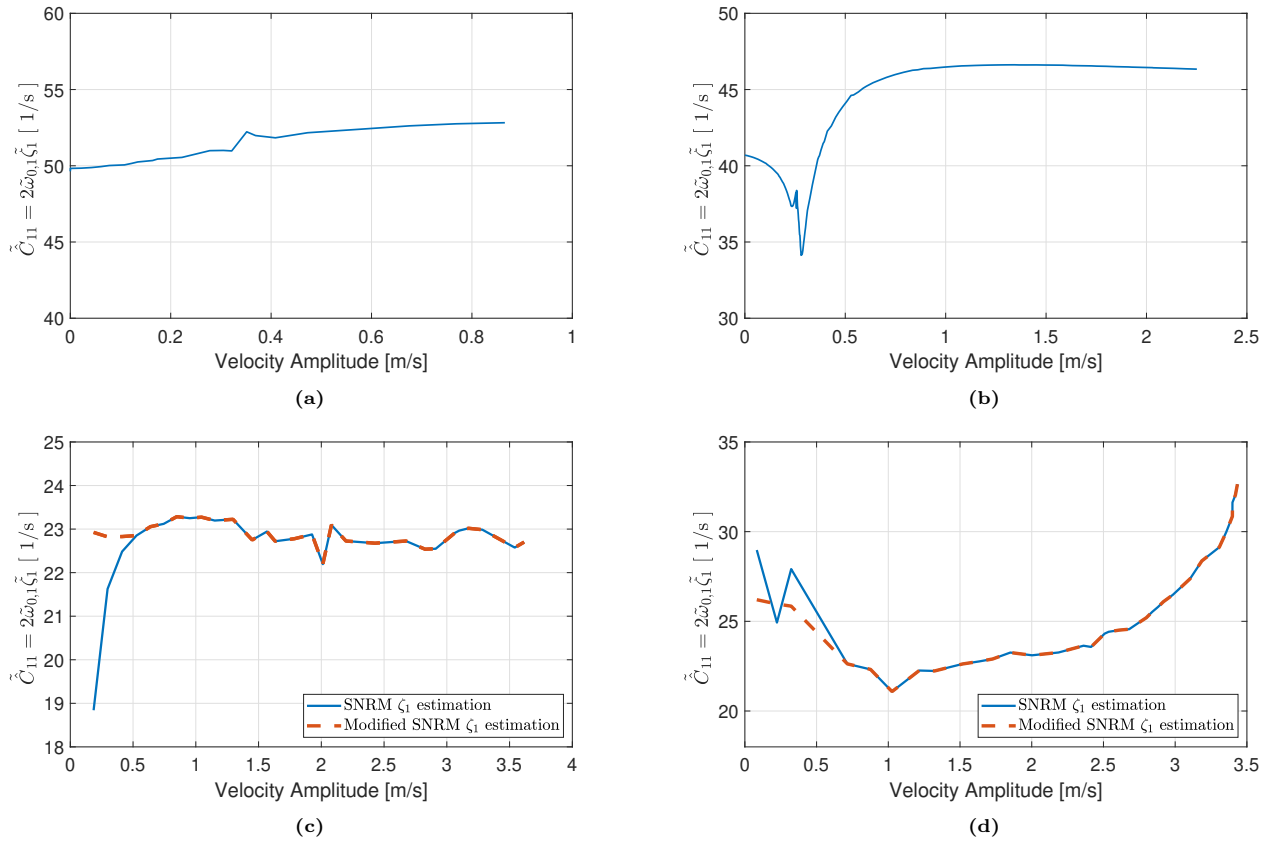

Fig. B.1: Modal damping computed for, respectively, numerical **(a)** flat and **(b)** curved, as well as, 3D-printed **(c)** flat and **(d)** curved beams.

This result was expected, since the ICE-ROM generated contains the nonlinearity solely in the stiffness part of its equation of motion, while the damping part is modeled as linear. In other words, matrix $\mathbf{C}$ in Eq. (B.1) is constant and thus $\tilde{\tilde{C}}_{11}$ should also be vibration-level-independent. Nevertheless, the modal viscous damping increases slightly with the vibration amplitude. This is most likely due to the fact that the inverse SNRM-based method estimates the NNM backbone to a satisfactory extent, but not perfectly. As presented in e.g. Fig. 8a, the estimated NNM backbone lays slightly above the true one computed with the Multi Harmonic Balance method. Recall that this SNRM-based algortihm assumes the solution to the nonlinear EOM in a form presented in Eq. (10), which is an approximation, thus the $\tilde{\tilde{C}}_{11}$ quantity is not guaranteed to be found as constant even in a numerical case study.

A similar result is obtained in case of the 3D-printed flat beam, whose modal viscous damping seems to be vibration-level-independent. It is worth noticing that the $\tilde{\tilde{C}}_{11}^{fb}$ function becomes horizontal after the nonlinear damping ratio function is tweaked manually to meet the ζ_1^{lin} when the vibration amplitude approaches zero. Without this adjustment there is a noticeable drop in the low amplitudes range, which is most likely non-physical. This study shows that the manual adjustment done to the nonlinear damping ratio curve might sometimes be necessary. It can also be claimed that the viscous damping corresponding to the first mode of vibration is approximately equal to 23.0 $\frac{1}{\mathrm{s}}$, see Eq. (B.3).

$$\tilde{\tilde{C}}_{11}^{fb} = 2\tilde{\omega}_{0,1}\tilde{\zeta}_1 \approx const = 23.0\ \frac{1}{\mathrm{s}}, \tag{B.3}$$

where the superscript fb stands for *flat beam*.

An interesting outcome is obtained in the cases of the numerical and 3D-printed curved beams. The simulated case study revealed a decrease of the modal damping when the beam exhibits softening. In the stiffening range, the $\tilde{\tilde{C}}_{11}^{cb}$ coefficient rapidly increases to approximately 47.0 $\frac{1}{\mathrm{s}}$ (which is higher than its linear C_{11}^{lin} value) and stays at this level when the motion amplitude keeps increasing. This result is at first glance very surprising because the nonlinearity is, once again, contained entirely in the stiffness part of the equation of motion. When it comes to the case with the 3D-printed curved beam (see Fig. B.1d), the modal damping also exhibits an initial decrease followed by an increase of its value. However, it is not as abrupt as in the numerical case study investigated. The authors suspect that this $\tilde{\tilde{C}}_{11}^{cb}$-amplitude-dependency is most likely caused by the

higher (or lower) harmonics present in the system's response, however this phenomenon requires more careful and in-depth investigation. On the other hand – the results on the *nonlinear* modal damping present in the flat beams are seemingly easy to interpret even with the simple formulas which are well-established in linear vibration theory.

References

[1] Raze, G., Guichaux, S., Jadoul, A., Broun, V., and Kerschen, G., 2020. "A Digital Absorber for Nonlinear Vibration Mitigation". In Proceedings of the 38th International Modal Analysis Conference (IMAC), Houston, TX, USA.

[2] Dogan, M. E., and Cigeroglu, E., 2020. "Vibration Reduction of a Structure by using Nonlinear Tuned Vibration Absorbers". In Proceedings of the 38th International Modal Analysis Conference (IMAC), Houston, TX, USA.

[3] Ehrhardt, D. A., Allen, M. S., Beberniss, T. J., and Neild, S. A., 2017. "Finite element model calibration of a nonlinear perforated plate". *Journal of Sound and Vibration,* **392**, pp. 280 – 294.

[4] Detroux, T., Kerschen, G., Ayme, F., Pavie, A., Osmond, G., and Lastere, N., 2020. "Nonlinear Ground Vibration Test of a Full-Scale Aircraft Horizontal Tail Plane". In Proceedings of the 38th International Modal Analysis Conference (IMAC), Houston, TX, USA.

[5] Rosenberg, R. M., 1960. "Normal Modes of Nonlinear Dual-Mode Systems". *Journal of Applied Mechanics,* **27**, pp. 263 – 268.

[6] Rosenberg, R. M., 1961. "On Normal Vibrations of a General Class of Nonlinear Dual-Mode Systems". *Journal of Applied Mechanics,* **28**, pp. 275 – 283.

[7] Rosenberg, R. M., 1962. "The Normal Modes of Nonlinear n-Degree-of-Freedom Systems". *Journal of Applied Mechanics,* **29**(1), 03, pp. 7–14.

[8] Rosenberg, R. M., 1966. "On Nonlinear Vibrations of Systems with Many Degrees of Freedom". *Advances in Applied Mechanics,* **9**, pp. 155 – 242.

[9] Cooke, C. H., and Struble, R. A., 1966. "On the existence of periodic solutions and normal mode vibrations of nonlinear systems". *Quarterly of Applied Mathematics,* **24**(3), pp. 177–193.

[10] Rand, R. H., 1971. "Nonlinear Normal Modes in Two-Degree-of-Freedom Systems". *Journal of Applied Mechanics,* **38**(2), 06, pp. 561–561.

[11] Rand, R. H., 1971. "A higher order approximation for non-linear normal modes in two degree of freedom systems". *International Journal of Non-Linear Mechanics,* **6**(4), pp. 545 – 547.

[12] Rand, R. H., 1973. "The geometrical stability of non-linear normal modes in two degree of freedom systems". *International Journal of Non-Linear Mechanics,* **8**(2), pp. 161 – 168.

[13] Rand, R. H., 1974. "A direct method for non-linear normal modes". *International Journal of Non-Linear Mechanics,* **9**(5), pp. 363 – 368.

[14] Manevich, L., and Mikhlin, I., 1972. "On periodic solutions close to rectilinear normal vibration modes". *Journal of Applied Mathematics and Mechanics,* **36**(6), pp. 988 – 994.

[15] Nayfeh, A., 1983. "The response of single degree of freedom systems with quadratic and cubic non-linearities to a subharmonic excitation". *Journal of Sound and Vibration,* **89**(4), pp. 457 – 470.

[16] King, M. E., and Vakakis, A. F., 1994. "An Energy-Based Formulation for Computing Nonlinear Normal Modes in Undamped Continuous Systems". *Journal of Vibration and Acoustics,* **116**(3), 07, pp. 332–340.

[17] Vakakis, A. F., Manevitch, L. I., Mikhlin, Y. v., Pilipchuk, V. N., , and A, Z. A., 1996. *Normal Modes and Localization in Nonlinear Systems.* Wiley.

[18] Vakakis, A. F., 1997. "Non-Linear Normal Modes (NNMs) and Their Applications in Vibration Theory: An Overview". *Mechanical Systems and Signal Processing,* **11**(1), pp. 3 – 22.

[19] Shaw, S., and Pierre, C., 1991. "Non-linear normal modes and invariant manifolds". *Journal of Sound and Vibration,* **150**(1), pp. 170 – 173.

[20] Shaw, S., and Pierre, C., 1993. "Normal modes for non-linear vibratory systems". *Journal of Sound and Vibration,* **164**(1), pp. 85 – 124.

[21] Peeters, M., Viguié, R., Sérandour, G., Kerschen, G., and Golinval, J.-C., 2009. "Nonlinear normal modes, part ii: Toward a practical computation using numerical continuation techniques". *Mechanical Systems and Signal Processing,* **23**(1), pp. 195 – 216. Special Issue: Non-linear Structural Dynamics.

[22] Noël, J., and Kerschen, G., 2017. "Nonlinear system identification in structural dynamics: 10 more years of progress". *Mechanical Systems and Signal Processing,* **83**, pp. 2 – 35.

[23] Pickrel, C. R., Foss, G. C., Phillips, A. W., Allemang, R. J., and Brown, D. L., 2006. "New Concepts GVT".

[24] Peeters, M., Kerschen, G., and Golinval, J., 2011. "Dynamic testing of nonlinear vibrating structures using nonlinear normal modes". *Journal of Sound and Vibration,* **330**(3), pp. 486 – 509.

[25] Kerschen, G., Peeters, M., Golinval, J., and Vakakis, A., 2009. "Nonlinear normal modes, Part I: A useful framework for the structural dynamicist". *Mechanical Systems and Signal Processing,* **23**(1), pp. 170 – 194. Special Issue: Non-linear Structural Dynamics.

[26] Szemplińska-Stupnicka, W., 1979. "The modified single mode method in the investigations of the resonant vibrations of non-linear systems". *Journal of Sound and Vibration,* **63**(4), pp. 475 – 489.

[27] Nayfeh, A., 1993. *Introduction to Perturbation Techniques.* Wiley Classics Library. Wiley.

[28] Peeters, M., Kerschen, G., and Golinval, J., 2011. "Modal testing of nonlinear vibrating structures based on nonlinear normal modes: Experimental demonstration". *Mechanical Systems and Signal Processing,* **25**(4), pp. 1227 – 1247.

[29] Ramlan, R., Brennan, M. J., Kovacic, I., Mace, B. R., and Burrow, S. G., 2016. "Exploiting knowledge of jump-up and jump-down frequencies to determine the parameters of a duffing oscillator". *Communications in Nonlinear Science and Numerical Simulation,* **37**, pp. 282 – 291.

[30] Peter, S., Scheel, M., Krack, M., and Leine, R. I., 2018. "Synthesis of nonlinear frequency responses with experimentally extracted nonlinear modes". *Mechanical Systems and Signal Processing,* **101**, pp. 498 – 515.

[31] Renson, L., Gonzalez-Buelga, A., Barton, D., and Neild, S., 2016. "Robust identification of backbone curves using control-based continuation". *Journal of Sound and Vibration,* **367**, pp. 145 – 158.

[32] Carrella, A., and Ewins, D., 2011. "Identifying and quantifying structural nonlinearities in engineering applications from measured frequency response functions". *Mechanical Systems and Signal Processing,* **25**(3), pp. 1011 – 1027.

[33] Carrella, A., 2012. "Nonlinear identifications using transmissibility: Dynamic characterisation of anti vibration mounts (avms) with standard approach and nonlinear analysis". *International Journal of Mechanical Sciences,* **63**(1), pp. 74 – 85.

[34] Arslan, O., Aykan, M., and Özgüven, H. N., 2011. "Parametric identification of structural nonlinearities from measured frequency response data". *Mechanical Systems and Signal Processing,* **25**, 05, pp. 1112–1125.

[35] Karaağaçlı, T., and Özgüven, H. N., 2021. "Experimental modal analysis of nonlinear systems by using response-controlled stepped-sine testing". *Mechanical Systems and Signal Processing,* **146**, p. 107023.

[36] Karaagacli, T., and Özgüven, H. N., 2021. "Experimental modal analysis of geometrically nonlinear structures by using response-controlled stepped sine testing". In Proceedings of the 39th International Modal Analysis Conference (IMAC), virtual.

[37] Karaağaçlı, T., and Özgüven, H. N., 2020. "Experimental identification of backbone curves of strongly nonlinear systems by using response-controlled stepped-sine testing (rct)". *Vibration,* **3**(3), pp. 266–280.

[38] Scheel, M., Kleyman, G., Tatar, A., Brake, M. R., Peter, S., Noël, J.-P., Allen, M. S., and Krack, M., 2020. "Experimental assessment of polynomial nonlinear state-space and nonlinear-mode models for near-resonant vibrations". *Mechanical Systems and Signal Processing,* **143**, p. 106796.

[39] Paduart, J., Lauwers, L., Swevers, J., Smolders, K., Schoukens, J., and Pintelon, R., 2010. "Identification of nonlinear systems using polynomial nonlinear state space models". *Automatica,* **46**(4), pp. 647 – 656.

[40] Dreesen, P., and M. Ishteva and, J. S., 2014. "Decoupling multivariate polynomials using first-order information". *SIAM Journal on Matrix Analysis and Applications,* **36 (2)**, pp. 864–879.

[41] Decuyper, J., Tiels, K., Runacres, M., and Schoukens, J., 2021. "Retrieving highly structured models starting from black-box nonlinear state-space models using polynomial decoupling". *Mechanical Systems and Signal Processing,* **146**.

[42] Newland, D., 1965. "On the methods of Galerkin, Ritz and Krylov-Bogoliubov in the theory of non-linear vibrations". *International Journal of Mechanical Sciences,* **7**(3), pp. 159 – 172.

[43] Hollkamp, J. J., Gordon, R. W., and Spottswood, S. M., 2005. "Nonlinear modal models for sonic fatigue response prediction: a comparison of methods". *Journal of Sound and Vibration,* **284**(3), pp. 1145 – 1163.

[44] Breitbach, E. J., 1973. "A semi-automatic modal survey test technique for complex aircraft and spacecraft structures". In Proceedings of the 3rd ESA Testing Symposium, p. 519–528.

[45] Wright, J., Cooper, J., and Desforges, M., 1999. "Normal-mode force appropriation—theory and application". *Mechanical Systems and Signal Processing,* **13**(2), pp. 217 – 240.

[46] Detroux, T., Renson, L., and Kerschen, G., 2014. "The harmonic balance method for advanced analysis and design of nonlinear mechanical systems". In Nonlinear Dynamics, Volume 2, G. Kerschen, ed., Springer International Publishing, pp. 19–34.

[47] Detroux, T., Renson, L., Masset, L., and Kerschen, G., 2015. "The harmonic balance method for bifurcation analysis of large-scale nonlinear mechanical systems". *Computer Methods in Applied Mechanics and Engineering,* **296**, pp. 18 – 38.

[48] Nayfeh, A., and Mook, D., 2008. *Nonlinear Oscillations.* Wiley Classics Library. Wiley.

[49] VanDamme, C. I., Moldenhauer, B., Allen, M. S., and Hollkamp, J. J., 2019. "Computing nonlinear normal modes of aerospace structures using the multi-harmonic balance method". In Nonlinear Dynamics, Volume 1, G. Kerschen, ed., Springer International Publishing, pp. 247–259.

[50] VanDamme, C. I., and Allen, M. S., 2018. "Using the harmonic balance method to directly compute NNMs of geometrically nonlinear finite element models". In Proceedings of the International Conference on Noise and Vibration Engineering (ISMA), Leuven, Belgium.

[51] Krack, M., and Gross, J., 2019. *Harmonic Balance for Nonlinear Vibration Problems.* Springer International Publishing, 03.

[52] Ehrhardt, D., Harris, R., and Allen, M., 2014. " Numerical and Experimental Determination of Nonlinear Normal Modes of a Circular Perforated Plate". In Proceedings of the 32nd International Modal Analysis Conference (IMAC), Orlando, FL, USA.

[53] Ehrhardt, D. A., Allen, M. S., and Beberniss, T. J., 2016. "Measurement of Nonlinear Normal Modes Using Mono-harmonic Force Appropriation: Experimental Investigation". In Nonlinear Dynamics, Volume 1, G. Kerschen, ed., Springer International Publishing, pp. 241–254.

[54] Ehrhardt, D. A., and Allen, M. S., 2016. "Measurement of nonlinear normal modes using multi-harmonic stepped force appropriation and free decay". *Mechanical Systems and Signal Processing,* **76-77**, pp. 612 – 633.

[55] Dassault Systèmes, 2018. SolidWorks. `https://www.solidworks.com`. Version 2018. Accessed: August 09 2019.

[56] Allen, M. S., and Ginsberg, J. H., 2006. "A global, single-input–multi-output (simo) implementation of the algorithm of mode isolation and application to analytical and experimental data". *Mechanical Systems and Signal Processing,* **20**(5).

[57] Kwarta, M., and Allen, M. S., 2020. "Nonlinear Normal Mode Estimation with Near-Resonant Steady State Inputs". In Proceedings of the 38th International Modal Analysis Conference (IMAC), Houston, TX, USA.